电 化 学
J. Electrochem. 2022, 28(2), 2108431 (1 of 24)

【Review】 **DOI**: 10.13208/j.electrochem.210843 **Http**://electrochem.xmu.edu.cn

Structural Degradation of Ni-Rich Layered Oxide Cathode for Li-Ion Batteries

Jia-Yi Wang[1,2], Sheng-Nan Guo[1], Xin Wang[2*], Lin Gu[1], Dong Su[1*]

(*1. Beijing National Laboratory for Condensed Matter Physics, Institute of Physics, Chinese Academy of Sciences, Beijing 100190, China; 2. School of Information and Optoelectronic Science and Engineering & International Academy of Optoelectronics at Zhaoqing, South China Normal University, Guangzhou 510006, Guangdong, China*)

Abstract: Nickel(Ni)-rich layered oxide has been regarded as one of the most important cathode materials for the lithium-ion batteries because of its low cost and high energy density. However, the concerns in safety and durability of this compound are still challenging for its further development. On this account, the in-depth understanding in the structural factors determining its capacity attenuation is essential. In this review, we summarize the recent advances on the degradation mechanisms of Ni-rich layered oxide cathode. Progresses in the structure evolution of Ni-rich oxide are carefully combed in terms of inner evolution, surface evolution, and the property under thermal condition, while the state-of-the-art modification strategies are also introduced. Finally, we provide our perspective on the future directions for investigating the degradation of Ni-rich oxide cathode.

Key words: lithium ion battery; cathode; Ni-rich layered oxide; structure evolution

1 Introduction

With the rapid development of portable electronic devices, energy storage stations and electric vehicles in recent years, the demanding for rechargeable secondary batteries is tremendous[1-7]. Compared with other energy storage systems, lithium-ion batteries (LIBs) hold advantages of high specific energy and high specific power, which have dominated the electronic and electrical markets since their first commercialization in 1990s[8-13]. Hopefully, next-generation LIBs can deliver even better performances as well as their energy density, power density, and cycle life[14-19].

A LIB consists of three main components, including cathode, anode, and electrolyte. At present, the cathode is the key component to improve the energy density, whose weight and cost account for 30% ~ 40% of the total battery[20-22]. In addition, the structure stability of cathode material significantly affects service life and safety of the whole battery[23]. In order to obtain LIBs with satisfying electrochemical performances, the candidate cathode materials are required to possess properties including high specific capacity, high redox potential, stable structure, small volume change in different cycling stages, fast Li^+/electron transport, good compatibility with electrolyte, abundant reserve, and low price, simultaneously[24].

During the past few decades, various cathode ma-

Cite as: Wang J Y, Guo S N, Wang X, Gu L, Su D. Structural degradation of Ni-rich layered oxide cathode for Li-ion batteries. *J. Electrochem.*, 2022, 28(2): 2108431.

Received: 2021-09-13, Revised: 2021-10-28. *Corresponding authors, Tel: (86-758)6635020, E-mail: wangxin@scnu.edu.cn, Tel: (86-10)8264955, dongsu@iphy.ac.cn

terials have been developed, such as $LiMn_2O_4$[25,26], $LiFePO_4$[27,28], $Li(Ni_xCo_yAl_{1-x-y})O_2$[29,30] (noted as NCA) and $Li((Ni_xCo_yAl_{1-x-y})O_2$[31-33] (noted as NMC), etc. For example, the 300 $Wh\cdot kg^{-1}$ cell-level energy milestone was lately achieved by Contemporary Amperex Technology (CATL) using NMC-811 cathode and Panasonic using NCA cathode[34]. Tesla Motors adopted an NCA cathode, $Li(Ni_{0.8}Co_{0.15}Al_{0.05})O_2$, in its Model S, which had a driving range of 270 miles[35]. Among them, NMC with high Ni content ($x \geqslant 0.5$) has received wide attentions due to its high specific capacity (more than 200 $mAh\cdot g^{-1}$), high average discharge voltage (~ 3.8 V vs. Li^+/Li) and relative low cost[36, 37]. Ni-rich NMC materials have a hexagonal layered structure (*R*-3m space group), similar to those of $LiCoO_2$. During the cycling process, Li ions can be extracted and inserted between the confined two-dimensional layers[38-42]. Up to date, Ni-rich NMC has become one of the most important cathode materials for LIBs due to its gravimetric capacity and cost efficiency[43]. However, NMC with high Ni content suffers from the fast structural failure and consequent safety issues[44,45]. To further improve the performance of NMC, the main challenge lies in the irreversible structural degradation during the cycling process, which eventually causes the fade of LIBs[30,31]. The present mechanisms can be summarized as following aspects: i) the microcracks originating from the anisotropic forces of the secondary particles, which cause the NMC bulk structure degradation. ii) the irreversible migration of Ni^{2+} to Li^+ site during the cycling process, inducing the generation of spinel/rock salt layer on the surface of NMC, which hinders the transport of Li^+ and electron. iii) the side reactions between NMC and the electrolyte, which gives rise to TM dissolution and phase conversion, producing huge impact on the structure stability and cycling performance. iv) the decreased thermal stability of NMC with the raised Ni content due to the strong oxygen release.

It is obvious that structural characterization on NMC structural evolution in the charge/discharge stages is crucial in understanding these aspects. Here, we present a comprehensive review focused on the structural failure mechanisms of NMC. As shown in Figure 1, the failure mechanisms can be elaborated from the internal structure evolution, the surface structure evolution and the structural degradation during thermal treatment. The strategies to improve the durability of Ni-rich NMC are also discussed, including heterogeneous ion doping, coating layer design, morphological control, and concentration gradient regulation. Finally, the prospections for future high-performance Ni-rich NMC cathode are put forward.

2 The Internal Structure Evolution in Ni-Rich Cathode

Internal microcracks caused by the mechanical stress has been regarded as one of the main reasons for the capacity decay in NMC materials, which results in the crush of the primary particles. The produced cracks are always accompanied with the generation of new electrolyte/NMC interface, where serious side reactions occur[49-52]. This section focuses on the microcracks originating from the NMC material interior according to the place where microcrack hap-

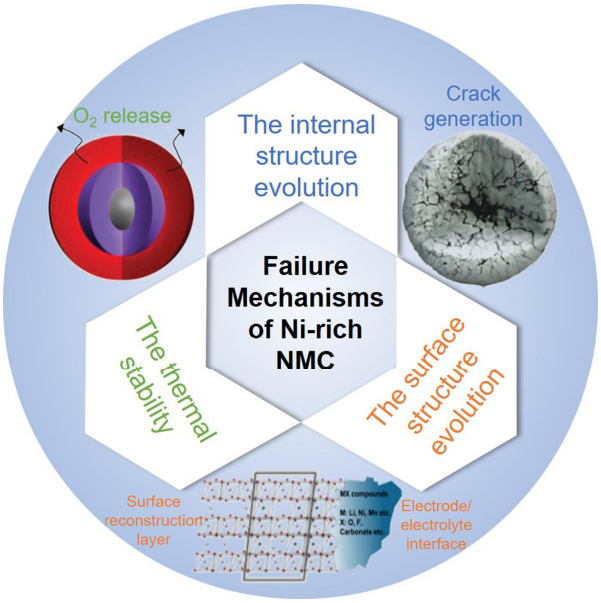

Figure 1 Illustration showing the failure mechanisms of Ni-rich NMC cathode. Reproduced with permission of Ref.[46], copyright 2020 Elsevier. Reproduced with permission of Ref.[47], copyright 2019 Wiley-VCH. Reproduced with permission of Ref.[48], copyright 2013 Wiley-VCH. (color on line)

pens (intergranular cracks and intragranular cracks).

2.1 Intergranular Cracks

In general, NMC materials deliver micron-sized microsphere morphology formed by the accumulation of nanoscale primary particles[24]. However, due to the volume change during the cycling process of the primary particles, stress accumulation will occur at the interfaces of these primary particles, eventually leading to the generation of intergranular cracks as shown in Figure 2(A)[46,53]. These microcracks are further aggravated during the repeated volume change in the cycling process, which significantly decreases the structural stability and electrochemical performance simultaneously. In order to further understand the large volume change during the cycling process, an *in situ* XRD experiment was conducted using $LiNi_{0.95}Co_{0.025}Mn_{0.025}O_2$ (NMC95) and $LiNiO_2$ (LNO) as cathodes by Yoon et al.[54] During the cycling process, the crystal structure of the NMC95 is transformed from hexagonal phase to monoclinic phase (H1→M), monoclinic phase to hexagonal phase (M → H2) and hexagonal phase to hexagonal phase (H2→H3) with the insertion and extracting of Li^+ in the crystal lattice, thus by the anisotropic changes along the *a*, *b* and *c* axes in the unit cell. At the initial stage of charging, the extracting of Li^+ leads to the increase of electrostatic repulsion between the adjacent oxygen layers, resulting in the increase of *c* axis. When fur-

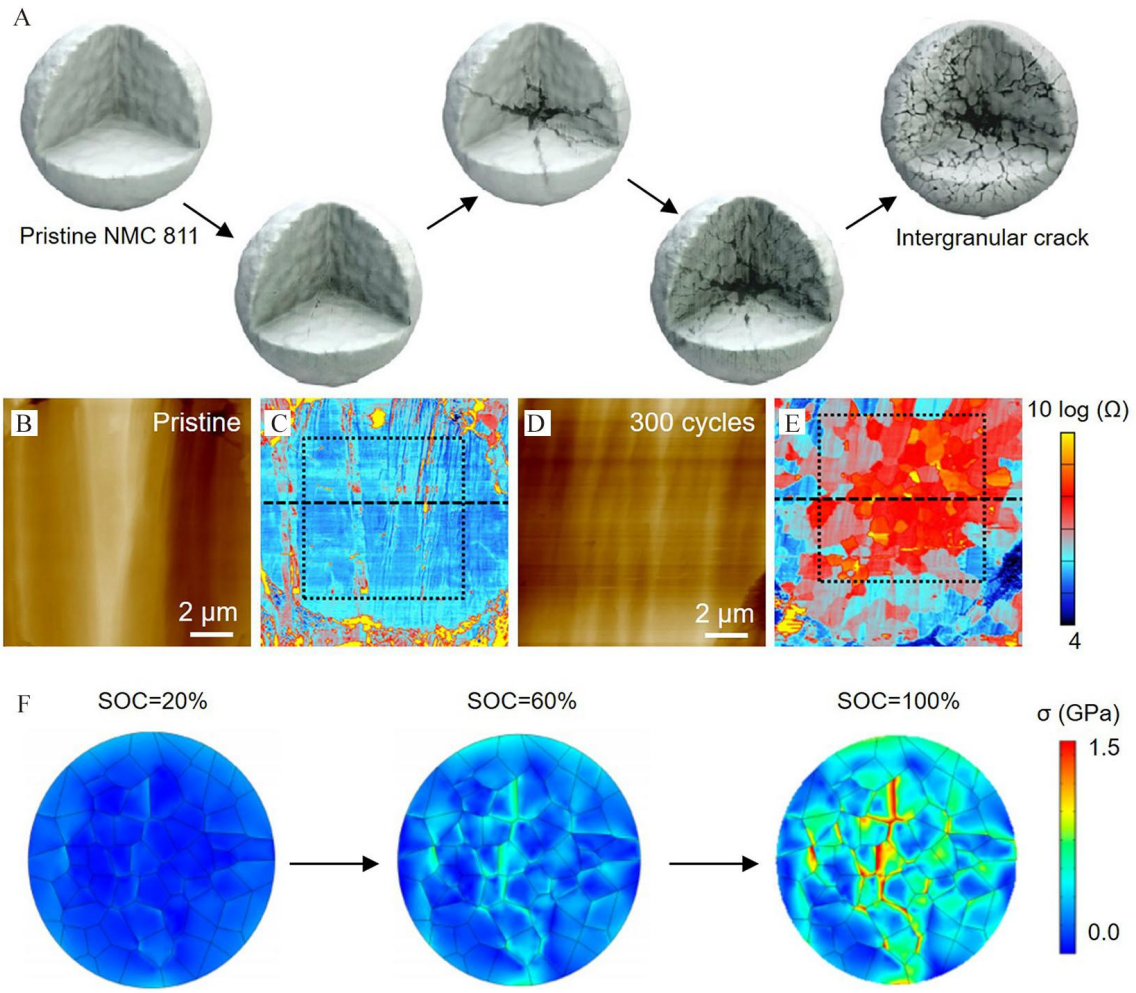

Figure 2 (A) The production of intergranular crack. Reproduced with permission of Ref.[46], copyright 2020 Elsevier. The (B, D) topographic and (C, E) corresponding Log(resistance) images at different stages of the sample. Reproduced with permission of Ref.[55], copyright 2018 Elsevier. (F) The stress distribution of NMC811 at different SOC values. Reproduced with permission of Ref.[56], copyright 2021 American Chemical Society. (color on line)

ther charging to 4.2 V, the excessive extracting of Li^+ causes the sharp contraction of layer spacing between the adjacent oxygen layers, resulting in the rapid decrease of c axis. Correspondingly, due to the continuous oxidation of transition metal ions during the charging process, the length along the a axis continues to be decreased. Finally, an obvious volume change ratio (~ 7%) is observed on NMC95 during the cycling process. Such produced anisotropic changes among the primary grain crystals can bring strong stresses at the disordered grain boundaries. In the constant cycling process, the repeated charge and discharge operations cause the constant change of the crystal lattice, which leads to the stress accumulation, thus by the generation of a large number of microcracks along the grain boundary. The contact between particles is impeded due to the generation of microcracks, thus leading to the rapid increase of electrical resistances, which is confirmed by Park et al. using scanning spreading resistance microscopy[55]. As shown in Figure 2(B-E), the cycled $LiNi_{0.8}Co_{0.15}Al_{0.05}O_2$ (NCA) particles demonstrated obviously different resistance distributions compared with the pristine NCA. Note that the observed electrical resistance in the cycled NCA was as high as four orders of magnitude than that in the pristine NCA, indicating the huge deterioration in electron transport due to the generation of microcracks.

The above discussion confirms the damage on the NMC materials brought by the microcracks. As a result, it is critical to probe the cause for the microcrack generation. Recent research indicates that the states of charge (SOC) is closely related to the production of intergranular cracks. Cheng et al. realized the visual observation of the microstructure change during the cycling process through *in situ* scanning electron microscopy (SEM)[56]. The obtained experimental results show that the microcracks of $LiNi_{08}Co_{0.1}Mn_{0.1}O_2$ (NMC811) particles are greatly affected by the working voltage window. At 4.1 V, it is not easy to produce microcracks inside the NMC811 particles. However, when the working voltage is increased to 4.7 V, microcracks can be found even in the initial cycle. The crack production originates from the center of the NMC811 particles and gradually extends to the surface. The finite element analysis demonstrates that the strengthened SOC can increase the stress distribution in NMC811 (Figure 2(F)). The randomly arranged grains in the core region of NMC811 produce relatively large mismatch strain, which cause higher stress concentration at the grain boundary. Under this high concentration of stress (> 1.5 GPa), the weak grain boundary is difficult to maintain stability, which leads to the initiation and propagation of intergranular cracks. This result is confirmed in Wu's work that chronic fatigue cracking was observed at low SOC, while drastic particle degradation happened at high SOC[57]. They found that cracks nucleation occurred at the end of charging and discharging leads to fast growth of cracks. The conclusion is consistent with Xu's description[58], higher charging voltage drives more Li ion extraction, which causes significant phase transformation and structure failure.

Apart from the SOC, the specific Ni content is also an important issue on the microcrack generation. In Ryu's work, $LiNi_{0.6}Co_{0.2}Mn_{0.2}O_2$(NMC622), NMC811, $LiNi_{0.9}Co_{0.05}Mn_{0.05}O_2$ (NMC955) and NMC95 were employed as cathodes to investigate the effect of Ni content[59]. As shown in Figure 3(A) and 3(B), the cathodes were all charged to 4.3 V and the corresponding SEM images were collected. A significant positive correlation can be observed between the number of microcracks and the Ni content. The NMC with higher Ni content reveals more anisotropic nature of the lattice, resulting in more H3 phase signals. The increased H3 content is harmful for the structure stability due to the accompanied disordered stress distribution, which can produce the anisotropic volume change, thus by the production of microcracks along the grain boundary. Furthermore, the particle fracture and fragmentation become progressively worse as the cycle continues. The focused ion beam-scanning electron microscope (FIB-SEM) was used by Miller et al. to probe the structure evolution with the increased cycle number[60]. The results as presented in Figure 3 (C) clearly confirm the deteriorative cracking and in-

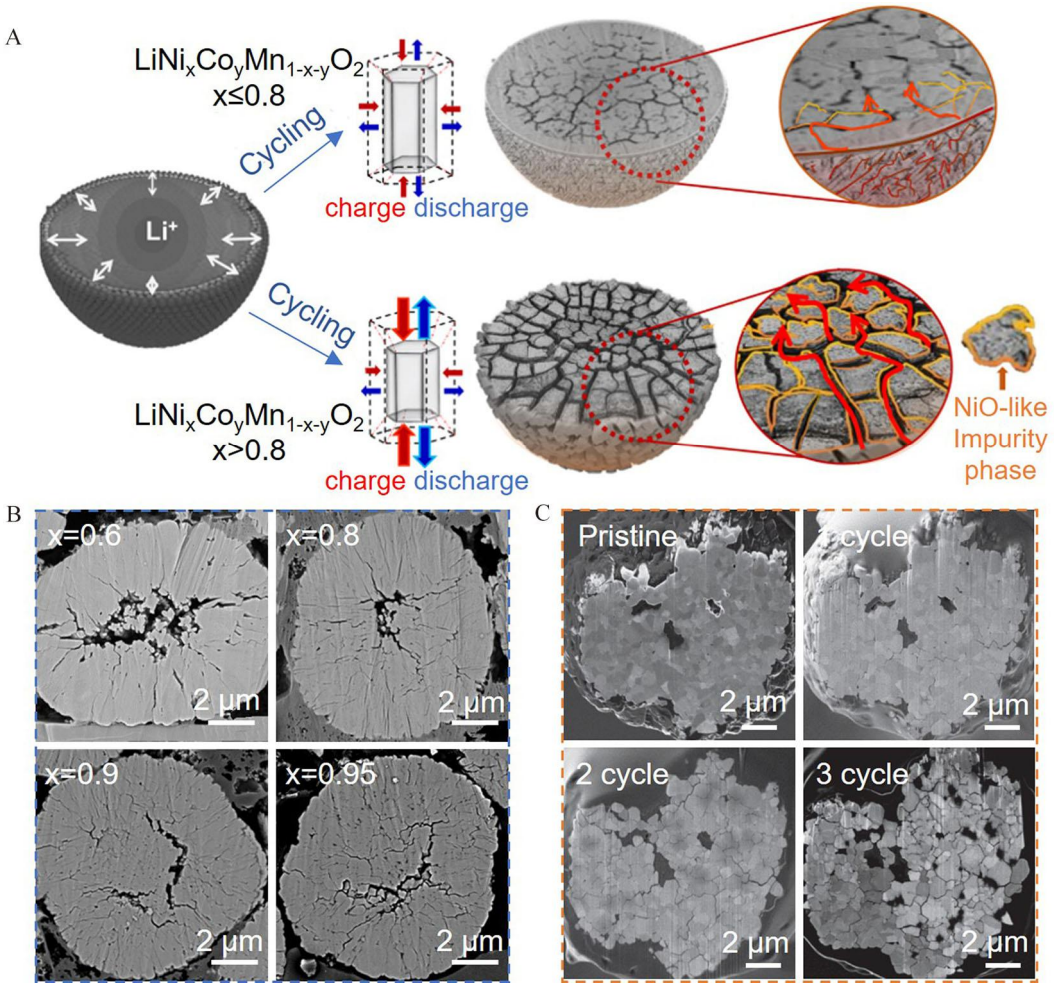

Figure 3 (A) Schematic diagram showing microcrack generation of NMC and (B) the corresponding SEM images of NMC with different Ni contents; Reproduced with permission of Ref.[59], copyright 2018 American Chemical Society. (C) SEM images of the cathode after different cycles. Reproduced with permission of Ref.[60], copyright 2013 Wiley-VCH. (color on line)

tergrain separation, which breaks the contact between the adjust grains. The phenomenon is also consistent with the significant initial capacity loss.

Combined with the above results, it is not difficult to find that the generation of microcracks is closely related to the production of H3 phase. For this purpose, the research progress to explore the transformation from H2 to H3 is summarized in this section. The *in situ* XRD is an effective method to monitor the phase transformation during the cycling process, which is also conducted by Li et al. As shown in Figure 4 (A), a typical phase change (H1 to H2, H2 to H3) is observed, which is consistent with the reported conclusion[37]. The peak shifts demonstrating the production of H3 phase is accompanied with the stretch and shrinkage on lattice parameter (a maximum variation of 0.478 Å along the *c*-axis, Figure 4(B) and 4(C)), which bring about the anisotropic nature among the grain boundary and following stress accumulation, thus by the final generation of microcracks. In addition, the solid state nuclear magnetic resonance (ss-NMR) experiments were employed by Zheng et al.[61], which can help us further understand the phase transformation from H2 to H3 phase. The ^{6}Li spin-echo *ex situ* ss-NMR spectra are displayed in Figure 4(D), the peak located at ~ 1400 ppm and ~ 150 ppm represent the Li atoms in the Li/Ni mixing state and perfect Li layer state, respectively. During the charging process, the negative peak shift means the Li^{+} extraction accompanied with the generation of H2 phase. The pro-

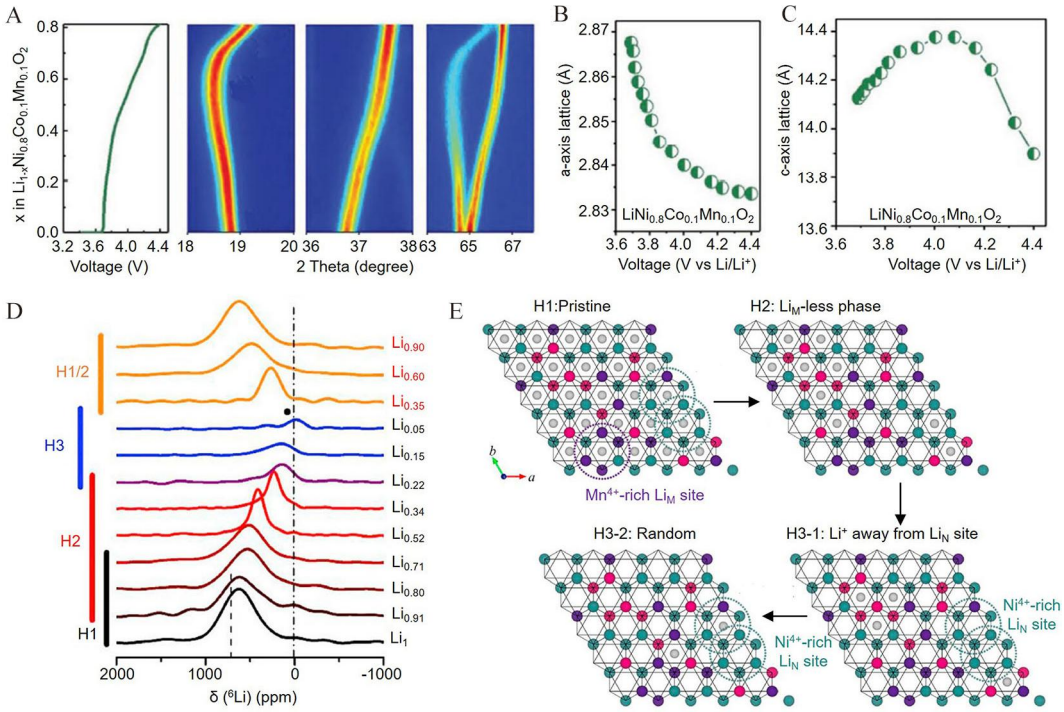

Figure 4 (A) *In-situ* XRD pattern of NMC811 cathode. Lattice changes of (B) *a*-axis and (C) *c*-axis as a function of voltage. Reproduced with permission of Ref.[37], copyright 2019 Wiley-VCH. (D) ^{6}Li spin-echo *ex-situ* NMR spectra of NMC811; (E) the schematic diagram of phase transformation along the *c*-axis. The grey, green, pink and purple balls represent Li, Ni, Co and Mn atoms, respectively. Reproduced with permission of Ref.[61], copyright 2019 Elsevier. (color on line)

duction of H3 phase can be observed from the $Li_{0.22}$ with the expansion of c-axis. According to the ss-NMR spectra, the possible evolution process is summarized as shown in Figure 4(E). The Li^+ located around Mn^{4+} (Li_M) is firstly exacted, which causes the production of H2 phase. After the complete Li_M extraction, two routines for Li^+ transport are proposed. The Li^+ located around Ni^{4+} (Li_N) firstly escapes to form H3-1 phase and a Li re-ordered state is put forward for the generation of H3-2 phase. In a word, the transformation from the H2 to H3 phase is the main reason for the stress accumulation, which causes the production of the microcracks in NMC materials.

2.2 Intragranular Cracks

Apart from the intergranular cracks, the microcracks yielded from the grain interior caused by the dislocation and uneven Li^+ diffusion also play an important role in the structure degeneration of NMC materials. Typical intragranular cracks can be seen in Figure 5(A)[62]. The classical term of crack is marked with a yellow arrow, featured with two adjusted parallel surfaces as a wedge-shape. This crack was developed along the (003) plane, which is always caused by the strong stress. The (003) intragranular cracking is regarded as the leading reason for the structure degradation, where the rock-salt phase was observed to be firstly grown[63]. The rock-salt phase hinders the delivery of stress in the layered structure, resulting in the fracture of the rock-salt lattice. The concentrated stress further boosts the nucleation and growth of the cracks, where finally a (003) crack is produced.

Furthermore, some dark contrasted strips can also be observed in Figure 5(A) (a pink arrow) with a widen plane space (0.6 ~ 0.8 nm), which is thought to be generated between two metal atom layers. Yan et al. speculated this crack to be a premature crack, which might be developed into a (003) crack as the cycle goes on. In order to verify this speculation, the atomic resolution scanning transmission electron micro scopic (STEM) and the corresponding annular bright-field

(ABF) images were collected and are shown in Figure 5(B) and 5(C). The black dots can be observed as labeled by the pink arrow, which indicated the generation of cationic ion mixing. The corresponding schematic diagram is described in Figure 5(D). In order to further disclose the role of dislocation, a dislocation in pristine NMC333 was surveyed (Figure 5(E)). The corresponding geometric phase analysis (GPA) demonstrates the strain distribution with a compressive and tensile lattice strain at the left and right sides, respectively (Figure 5(F)). Figure 5(G) performs the schematic diagram of the whole dislocation, the produced strain field can affect more than 100 nm, which can make a contribution to the generation of final microcracks.

In addition to the dislocation, the nonuniform Li^+

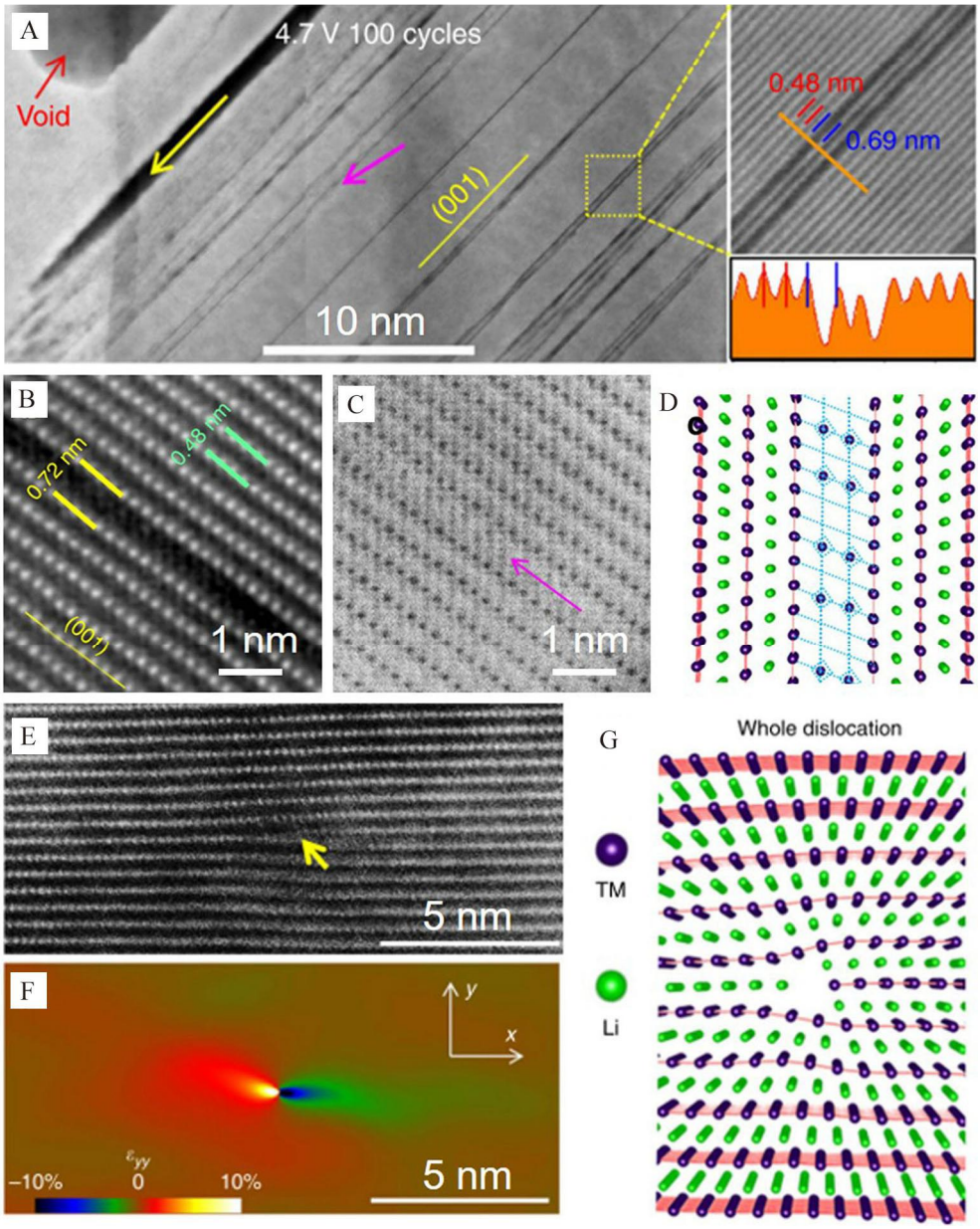

Figure 5 (A) STEM image of cycled NMC333 particles; (B) the atomic resolution STEM image and (C) the corresponding ABF image along [010] axis; (D) the corresponding schematic diagram; (E) the STEM image of NMC333 and (F) the corresponding strain map; (G) the corresponding schematic diagram. Reproduced with permission of Ref.[62], copyright 2017 Nature Publishing Group. (color on line)

diffusion is another reason for the intragranular cracks production. Stable and uniform Li^+ diffusion process is vital for the battery design with high cycling stability. The irreversible phase change, stress concentration, crack and even particle rupture can be observed when the uniform Li^+ diffusion cannot be maintained, which can cause the irreversible capacity decay. Therefore, the diffusion behavior of Li^+ is an important fundamental issue needed to be explored. However, due to the light weight of Li, it is difficult to conduct the visualization research relying on current technologies with limited resolution. These issues hinder the researchers to profoundly investigate the accurate Li^+ diffusion behaviors. In order to address this problem, Xiao et al. was inspired by the prosperous sodium (Na) ion battery[64]. Compared with Li, Na delivers larger size and higher mass, which can be detected by current TEM. Therefore, the Na^+ was in jected relying on sodiating the delithiated NMC333, which was employed to trace the routine of Li^+ diffusion. Two types of Na^+ diffusion were delivered. One typical diffusion can be observed along the (003) plane (denoted as L-type), which was confirmed by the HAADF image and the corresponding element distribution (Figure 6(A) and 6(B)). This distribution pattern was characterized by the striped dis-

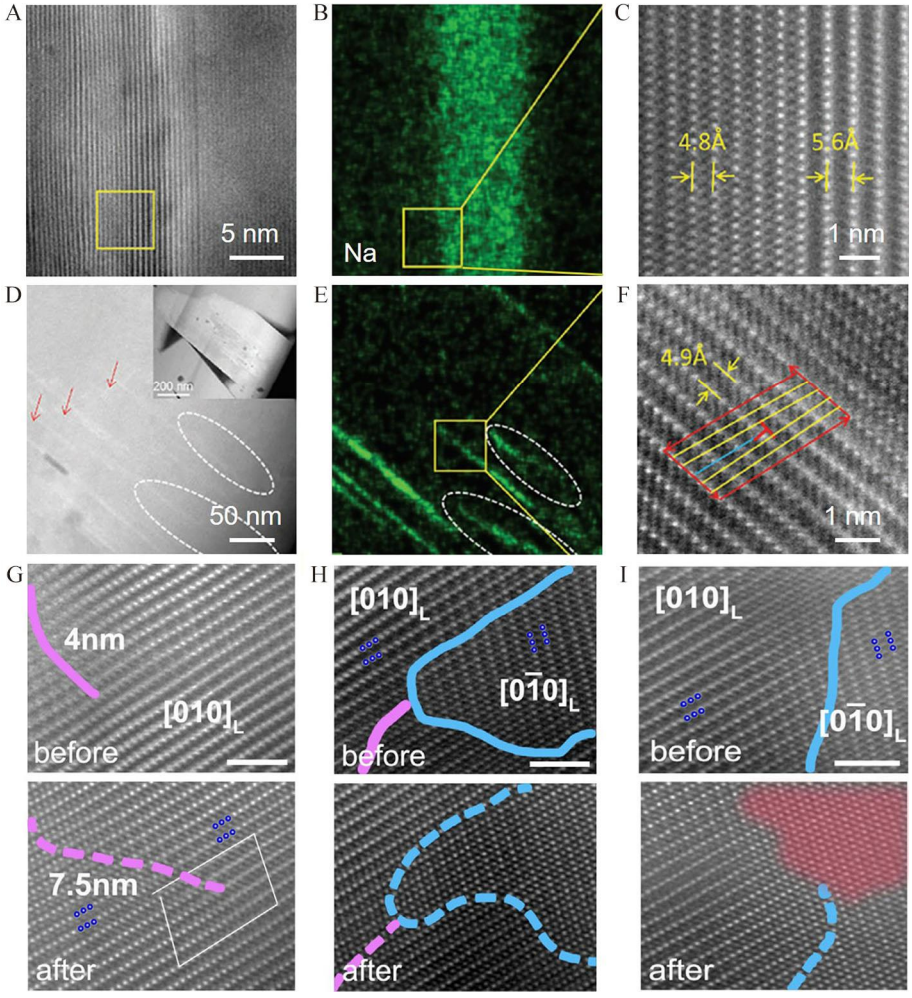

Figure 6 (A) The HAADF-STEM image, (B) Na element distribution of the selected area, (C) the atomic distribution of the selected area with L-type ion diffusion. (D) The HAADF image, (E) the Na element distribution, (F) the atomic distribution of the selected area with D-type ion diffusion. Reproduced with permission of Ref.[64], copyright 2019 Wiley-VCH. The STEM images with (G) pure APB, (H) APB and TB, and (I) TB before and after the delithiation. Reproduced with permission of Ref.[65], copyright 2020 Wiley-VCH. (color on line)

tribution of Na^+ and was connected to the grain edge, which was consistent with the conventional Li^+ diffusion along the (003) plane. Due to the larger ion radius of Na^+, the layer spacing was expanded from the initial 4.8 Å to 5.6 Å, which was the typical layer spacing of P3 type sodium containing layered cathode materials (Figure 6(C)). The other diffusion path occurred along the dislocations (denoted as D-type), where Na^+ showed a random distribution. In this type, the Na^+ diffusion tendency was not only along interlayer, but also across layer, and the distribution of Na^+ did not show a continuous banded trend (Figure 6(D) and 6(E)). Further analysis in the crystal structure of the sodium-rich region showed that the Burger's circuit could not be closed, indicating that there was a dislocation in the region (Figure 6(F)). The GPA of the region showed that there were more than 20% strains in the dislocation center. The most significant difference between D-type distribution and L-type distribution was that the entry of Na^+ did not significantly increase the size of layer spacing. Although the size of Na^+ was larger, the existence of dislocations may prevent the layer spacing from expansion. As a result, the change of layer spacing was a direct criterion to judge the diffusion path of Na^+ that largely reflected the escape path of Li^+. Therefore, in the early stage of lithiation, Li^+ prefers to be diffused into the NMC particle along the defect path. After that, Li^+ enters the interior of the NMC particle through the routine along the (003) crystal plane. Significant inhomogeneity exists in the ion diffusion process, which can cause the production of intragranular cracks.

Above research confirms the relation between the dislocation and the heterogeneous Li^+ diffusion. As a result, it is necessary to investigate the crystallographic defect structure in the NMC materials. In order to visualize the crystallographic defects (including dislocations, stacking faults, antiphase boundaries, and twin boundaries) evolution during the cycling process, Li et al. constructed a solid-state battery using the $LiNi_{0.76}Mn_{0.14}Co_{0.10}O_2$ (NMC76) as a cathode and $Li_{0.5}La_{0.5}TiO_3$(LLTO) as a Li^+ donor inside TEM[65]. Three phases (layered, spinel and rock-salt) and five phase boundaries (layered/layered phases (APB), twin boundary between layered phases (TB), layered/spinel phases, rock-salt/spinel phases and rock-salt/layered phases) were observed. The typical APB (the magenta line) and TB (the blue line) boundaries are shown in Figure 6(G-I). Obvious extension can be observed around APB after delithiation as shown in Figure 6(G). In addition, a detectable TB movement along the (003) plane was performed in Figure 6(H) as well as the enlarged Li/Ni mixing area around TB in Figure 6(I). The results of density functional theory (DFT) demonstrated that the TB boundary provided a feasible diffusion channel with a reduced energy barrier for Li^+ and transition metal atoms, which can promote the formations of cationic disorder and rock-salt phase. Structurally, the proliferation of APB blocked the Li^+ diffusion channel, possibly leading to an impedance increase in the lithiation/delithiation process. The nonuniform diffusion of Li^+ and the migration of transition metal ions caused by defects in the NMC particles have important effects for the structure degradation.

In view of the above results, the single-crystal NMC was developed and is expected to relieve the negative effect of cracks relying on the reduced phase boundaries and material surfaces compared with its polycrystalline counterpart. The "single-crystal" feature restricts the surface reactivity as well as particle cracking, leading to the enhanced service life. Qian et al. proved that the electrochemical performance can be significantly enhanced by eliminating the internal grain boundaries and inter-granular fracture by employing the single-crystal NMC622 cathode[66]. However, there was still serious kinetic limitation found on the single-crystal NMC, which hinders its practical implementation. Trevisanello et al. compared the electrochemical behaviors of single-crystal NMC and corresponding polycrystalline counterpart[67]. Although secondary particle cracking can be observed in the polycrystalline sample, liquid electrolyte infiltration into the cracks brings obviously improved diffusion coefficient. While "uncracked" single-crystal NMC is still suffered from the severe ion diffusion limitations

companied with low capacity. Therefore, morphology and size optimization of single crystalline NMC are crucial for available Li chemical diffusion coefficient. Apart from the single crystal design, the grain boundary modification is also an effective routine to weaken the influence of cracks. Yan et al. infused Li_3PO_4 into the grain boundaries of NMC76, which was reported to significantly improve the longterm cycle stability of both capacity and voltage[68]. This grain boundary modification addresses several issues including the solid-liquid interfacial problem, intergranular cracks and detrimental phase change.

3 The Surface Structure Evolution in Ni-Rich Cathode

In recent years, much efforts have been devoted to find out the degradation mechanism of NMC surface during the cycling process[69, 70]. A typical phase transformation from layered structure to spinel structure and then to rock-salt phase is recognized as shown in Figure 7(A)[47,71,72]. Lin et al. used $LiNi_{0.4}Mn_{0.4}Co_{0.18}Ti_{0.02}O_2$ (NMCT) as a cathode to supervise the surface structural reconstruction and chemical evolution in the cycling process[73]. The clear layered structure and accurate atomic site occupation can be seen in Figure 7 (B). After the cycles, an observable surface reconstruction layer is demonstrated in Figure 7(C). Combining the FFT patterns, the reconstruction layer was composed mainly of rock-salt phase as well as some spinel phases connecting the layered phase and rock-salt phase. In addition, based on Jung's work[74], this transformation would be intensified under the

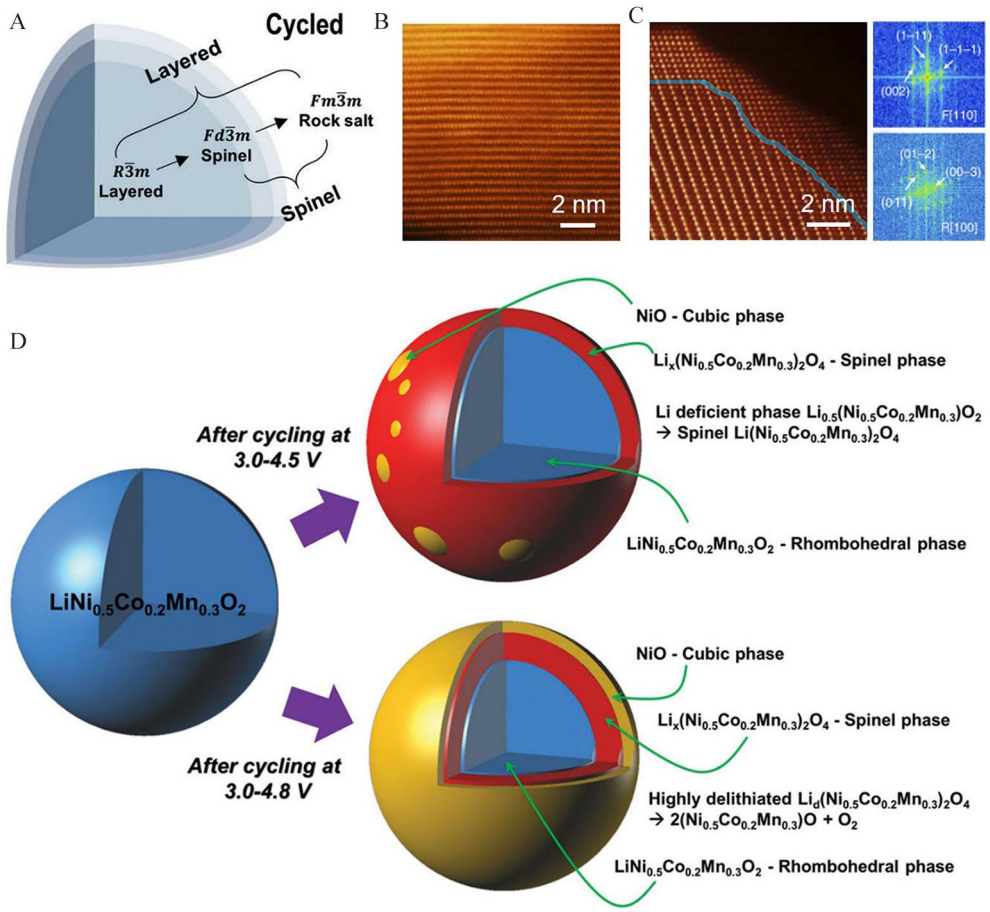

Figure 7 (A) Typical phase transformation schematic diagram. Reproduced with permission of Ref.[47], copyright 2019 Wiley-VCH. (B) The high-resolution STEM images of (B) pristine and (C) cycled NMCT particle as well as FFT patterns for the layered and reconstruction part. Reproduced with permission of Ref.[73], copyright 2014 Nature Publishing Group. (D) the structure evolution of NMC cathode under different voltages. Reproduced with permission of Ref.[74], copyright 2014 Wiley-VCH. (color on line)

highly delithiated state. Under 4.5 V cutoff voltage, the cycled NCM523 particles delivered dominating spinel phase with some rock salt formation. When the cutoff voltage was increased to 4.8 V, a sandwich structure (rock salt phase-spinel phase-layered phase) can be observed after cycling (Figure 7(D)). Noting that the phase transformation occurred in a surface region around 15 ~ 20 nm, which was not affected by the cutoff voltage. The studies have shown that the Li/Ni mixing is a crucial driving force for the phase transformation. The Ni atom in Ni-rich NMC material delivers two valence states: +2 and +3. According to the crystal field theory, Ni^{3+} in octahedral position is unstable due to the presence of unpaired electrons in e_g electron orbit, and tends to be Ni^{2+}. However, due to the close ion radii of Li^+ (0.76 Å) and Ni^{2+} (0.69 Å), Ni^{2+} will be migrated from the 3a position to the 3b position in the lattice during the preparation process and the cycling process, resulting in cation mixing.[10] In the case of $LiNiO_2$, the layered phase is, as calcu lated, transformed into the spinel phase when 25% Ni^{2+} is mixed in the 3b position[75]. As the Ni^{2+} mixed percentage is increased to 50%, the rock-salt phase can be observed. The Ni atoms in the spinel and rock salt phases deliver electrochemical sluggishness, which would hinder the Li ion migration.

Above mentioned structure degradation relating to the transformation from layered structure to spinel structure and then to rock-salt phase would take place during the initial cycling process. The structure evolution throughout the whole cycling process is also necessary for the further understanding. Lin et al. employed STEM test to inquire the structural transformation and chemical evolution of NMC811 during the long cycling process[76]. Compared with the pristine layered phase (Figure 8(A)), obvious phase transformation occurred at the 20th cycle (Figure 8(B)) and the transformation depth was gradually increased along with the cycle going on (Figure 8(C)). Noting that the pristine smooth surface is trans formed into zigzag after 100 cycles (Figure 8(D)). At the same time, the atom rearrangement is confirmed relying on the continuously acquired SAED patterns during the cycling process. For the further analysis of atom arrangement, a NMC811 particle after 100 cycles was used to conduct the fine structure exploration. Four phases are observed including layered phase (Figure 8(E)), disordered layered phase (Figure 8(F)), defect rock salt (Figure 8(G)) and rock salt phase (Figure 8(H)). This is due to the continuous migration of metal cations into the Li^+ sites, and the layered structure of the surface region is gradually transformed into the electrochemically inert rock salt phase as well as the formation of disordered layered and defective rock salt phase. Among the metal cations, Ni ions play an important role during the process of structural evolution. Ni ions migrate from the granular phase to the outer surface along the diffusion direction of Li^+, accompanied by irreversible reduction reaction. This atomic rearrangement leads to a structural transformation that ultimately reduces the capacity of the battery. Furthermore, due to the low diffusion barrier of Ni in the lithium layer and the presence of Ni concentration gradient in the crystal lattice, the migration of Ni ions will run through the whole cycle, leading to the continuous degradation of the electrochemical performance.

The surface reconstruction of Ni-rich cathode and the resulting capacity attenuation have been recognized by researchers[77, 78]. Xu et al. demonstrated that the Li/Ni antisite mixing enhancement was observed from the pristine state to 1200 ageing cycles[79]. Due to the electrochemically inactive nature of the rock salt phase on the surface of NMC811, the crystal structure remains nearly unchanged during the cycling process, while the layered phase exhibits considerable lattice expansion and contraction. As a result, NMC811 particles produce dynamic lattice mismatches between the rock salt phase and the layered phase, which is also related to the relative orientation of the two structures. When NMC811 is in the SOC above ~ 75%, high lattice strain between the rock salt and layered phase can be observed as speculated from the variation of value of *a*/*b*/*c* axis (Figure 8(I)). The structural evolution of NMC811 with thin or no

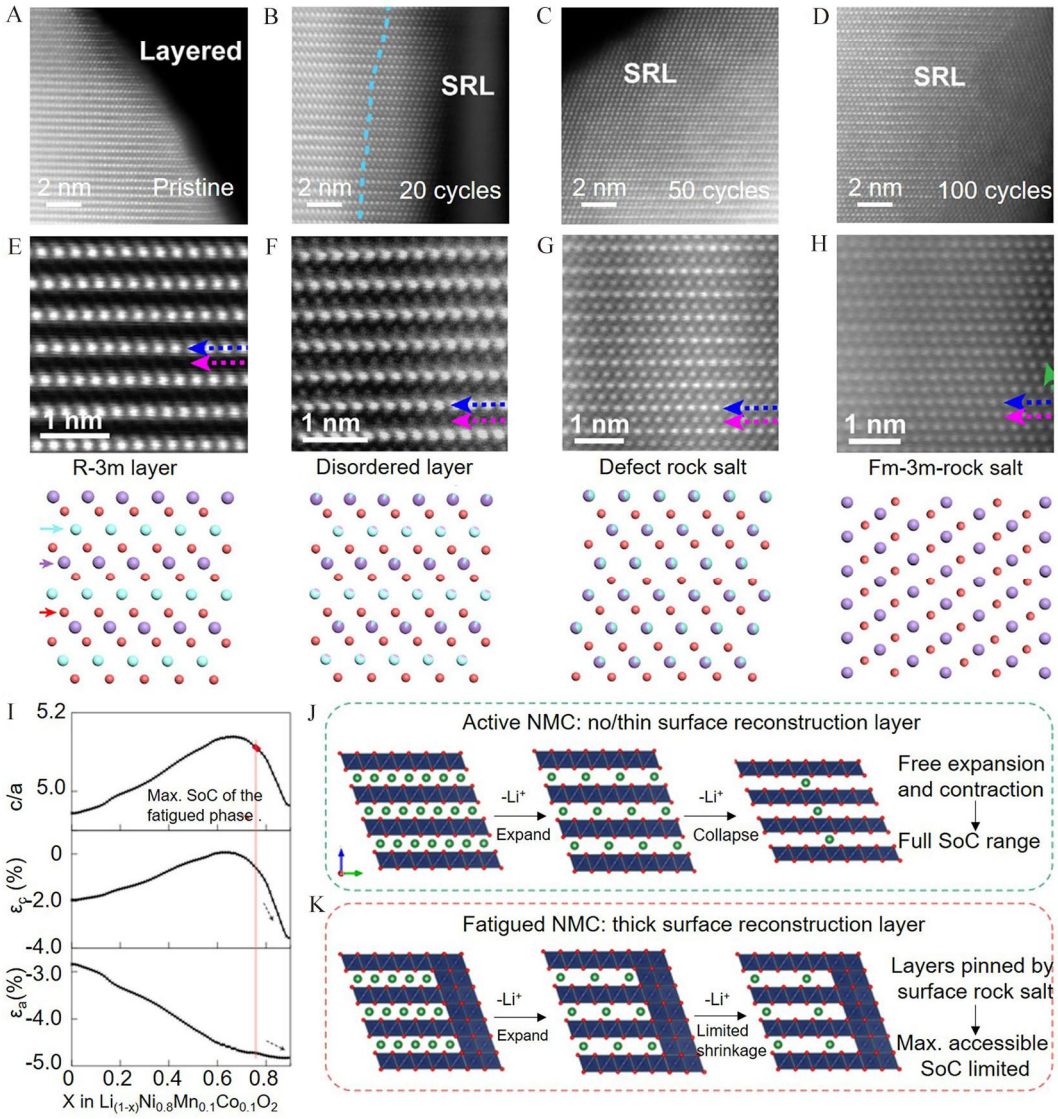

Figure 8 STEM images of NMC811 after (A) 0 cycle, (B) 20 cycles, (C) 50 cycles and (D) 100 cycles. The STEM image of NMC811 at different regions including (E) layered phase; (F) disordered layered phase; (G) defect rock salt phase and (H) rock salt phase. Reproduced with permission of Ref.[76], copyright 2018 Elsevier. (I) the spacing ratio of the *c* direction and *a* direction; the lattice mismatch in the *c* and *a* directions; the schematic diagram showing structures of the (J) active NMC811 and (K) fatigued NMC811. Reproduced with permission of Ref.[79], copyright 2021 Nature Publishing Group. (color on line)

rock salt surface indicated that the unit cell lattice can be expanded and contracted freely, which can be realized in the SOC range from 0 to 100% (Figure 8 (J)). However, a thick surface reconstruction layer hinders the volume change of NMC811 in the cycling process due to the high lattice mismatch, which limits the SOC value (Figure 8(K)).

In addition to the surface reconstruction, the side reactions occurred in the electrode-electrolyte interface are also great challenges for the further development of Ni-rich cathode materials. The interfacial side reactions mainly include the decomposition of electrolyte, dissolution of transition metal ions, generation of transition metal oxides, and formation of solid-electrolyte interface (SEI) (Figure 9(A))[47], which reduce the stability of the interface, thus affecting the migration and diffusion of Li^+. Ideally, the operating voltage window of the battery should be between the highest occupied molecular orbital (HUMO) and lowest unoccupied molecular orbital (LUMO) of the elec-

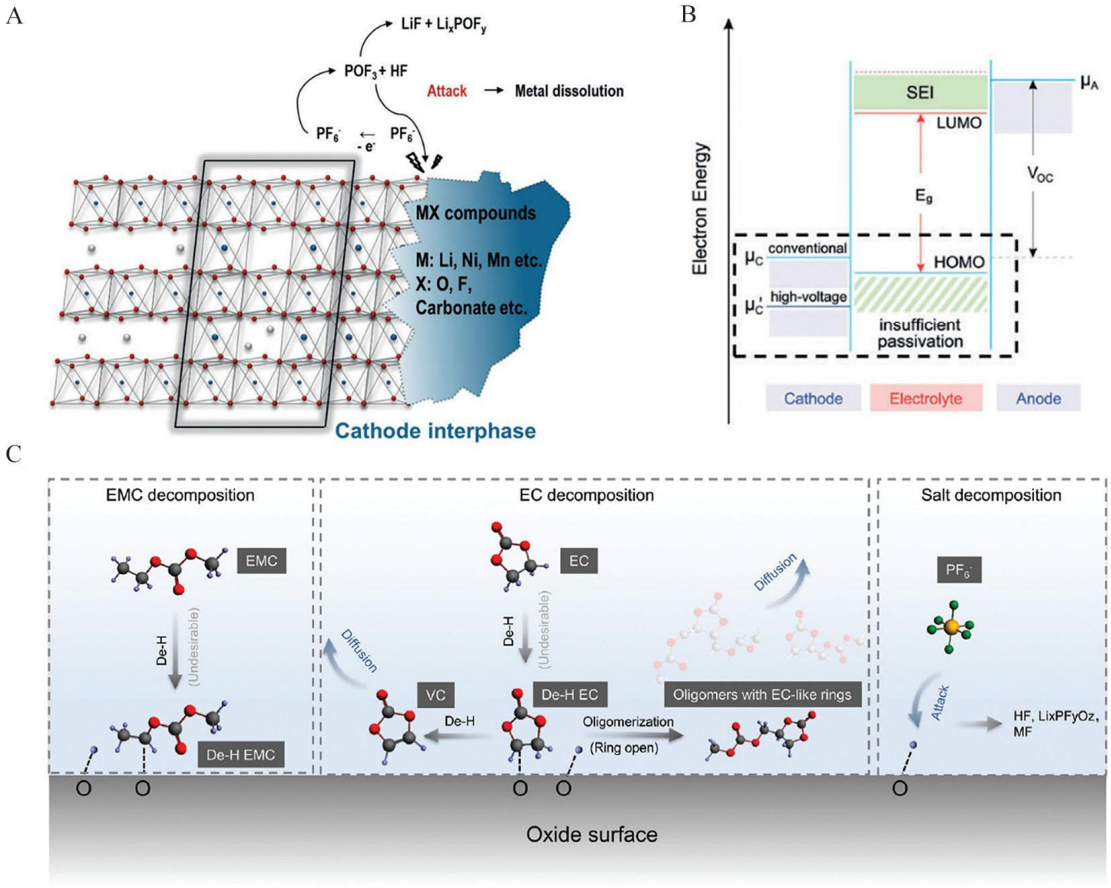

Figure 9 (A) The schematic diagram of the side reactions in the electrode-electrolyte interface. Reproduced with permission of Ref.[47], copyright 2019 Wiley-VCH. (B) the relation between anode/cathode working voltage and the energy level of electrolyte. Reproduced with permission of Ref.[80], copyright 2017 Royal Society of Chemistry. (C) the electrolyte decomposition mechanism on NMC811. Reproduced with permission of Ref.[81], copyright 2020 Royal Society of Chemistry. (color on line)

trolyte[80]. At this point, the electrolyte simply acts as an inert Li^+ transport medium. However, due to the pursue for high capacity, current batteries often need to be operated under wide voltage window (beyond the HUMO and LUMO of current organic electrolyte, Figure 9(B)), which lead to the breakdown of the electrolyte. After the electrolyte is decomposed, further reactions with the cathode material would occur, thus by the loss of the active material as well as Li^+. Many interaction mechanisms between NMC surface and electrolyte have been present including nucleophilic attack reactions, electrophilic attack as well as dehydrogenation reactions[81]. It should be noted that the interaction is strengthened under the raised Ni content in NMC materials, which is attributed to strong metal-oxygen bonding and increased oxygen p states pinned at the Fermi level[82]. Zhang et al. employed *in situ* FT-IR method to explore the chemical structure evolution and proposed detailed working mechanism between the electrolyte and NMC811 as shown in Figure 9(C)[81]. EMC reacted with the NMC811 relying on the C-O bond after b-site hydrogen dissociation. Similar dehydrogenate reaction can be seen on the EC that can be further dehydrogenated to form VC. Another evolution possibility is also put forward: the de-H EC can react with the surface oxygen on the NMC811 to produce oligomers. In addition, the passivating layer is generated due to the carbonate decomposition, inducing the increased impedance. Although several efforts have been devoted to prevent the side reactions in order to enhance the surface structure stability of Ni-rich cathode materials, there

is a long way to go before its practical implement.

4 The Thermal Stability of Ni-Rich Cathode

Safety is the first premise for many applications of LIBs. Ni-rich cathode materials have been suffering from low thermal stability, which reduce the cycling stability and even cause the collapse of the whole battery system[83-85]. It is noted that the thermal stability will be decreased with the increase of Ni content as shown in Figure 10(A)[86]. Being charged to 4.3 V, the decomposition temperatures of NMC111, NMC523 and NMC811 were 306 ℃, 290 ℃ and 232 ℃ respectively. The highly charged state may cause the release of oxygen, which would react with the electrolyte. Bak et al. used an *in-situ* technique that combined time-resolved X-ray diffraction and mass spectroscopy (TR-XRD/MS) to explore the structure evolution and gas release during the heating process[87]. As shown in Figure 10(B), the first transformation from the layered phase to the spinel phase occurred at about 194 ℃, and followed by the change to the rock-salt phase from 275 ℃ to 500 ℃. Apart from the phase transition, the MS patterns delivered two O_2 production peaks at about 240 and 320 ℃, which was related to the two phase transformation stages from the layered to the spinel and then to the rock salt phases. In addition, a continuous CO_2 release signal was observed from 250 ℃ to 500 ℃ and a peak value was found at about 380 ℃, which was later than the O_2 release. These results are also confirmed by Li's work and detailed working mechanisms are also provided (Figure 10(C-E))[88]. With the temperature going up, the existence of lattice oxygen changed into the forms of $O_2^{2-}/O^{2-}/O^-$, which were chemically adsorbed in the lattice positions. Ideally, higher temperature drove the transformation into O_2, thus reacting with the electrolyte. However, the $O_2^{2-}/O^{2-}/O^-$ always immediately reacted with the electrolyte as well as

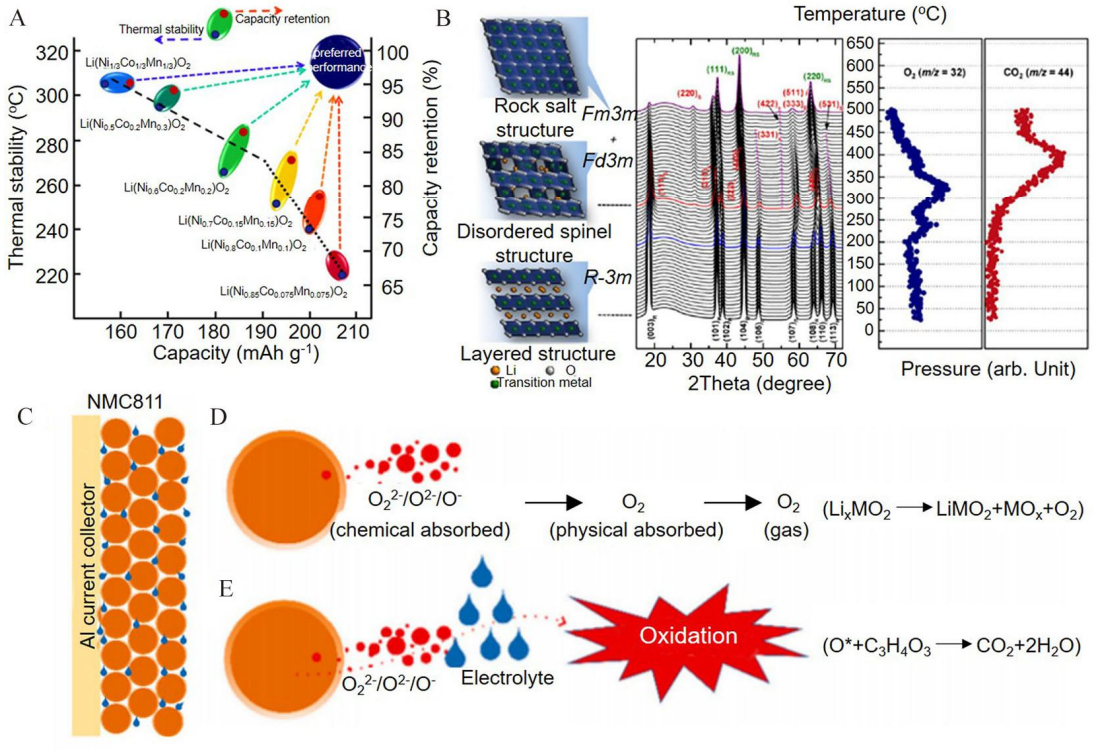

Figure 10 (A) the relationship of thermal stability, capacity and capacity retention. Reproduced with permission of Ref.[86], copyright 2013 Elsevier. (B) TR-XRD/MS patterns. Reproduced with permission of Ref.[87], copyright 2013 American Chemical Society. (C-E) the cathode component illustration and the possible reaction mechanisms. Reproduced with permission of Ref.[88], copyright 2021 Elsevier. (color on line)

abundant heat release in a real battery system. More seriously, the released heat further aggravated the thermal run away of the whole battery system.

With the development of advanced characterization technologies, structural evolution of NMC during the heating process are observed. Alvarado et al. employed the synchrotron radiation characterization to investigate the thermal behaviors of NMC811[89]. The *ex-situ* thermal studies using hard X-ray absorption spectroscopy indicated that the delithiated NMC811 delivered an initial elevated oxidation state of Ni/Co until 120 °C. As the temperature being further raised, the valence states of Ni/Co started to fall. The authors speculated that the oxidation stage was caused by the Ni/Co-O bond variation in covalencies or bond lengths instead of true oxidation. Different from Ni/Co, the valence state of Mn kept constant at tetravalent state during the heating process, indicating the excellent thermal stability. In addition, the three-dimensional XANES results indicated that the NMC811 particles with large size possessed higher thermal stability.

Crack induced structural degradation is a critical issue. Its evolution under thermal condition is also an important field that needs to be explored. Mu et al. investigated the structure transformation of delithilated $LiNi_{0.4}Mn_{0.4}Co_{0.2}O_2$ (NMC442) particle under thermal run away activation using *in situ* environmental TEM[90]. As shown in Figure 11(A), no obvious cracks can be seen before thermal activation. After heating 230 °C for 12 min, some slender microcracks were produced, which grew quickly with the prolong of heating time. A crack nearly across the whole particle was delivered at 40 min, which was thought to be generated along the grain boundary. After that, the finite element modeling (FEM) was conducted to explain the reason for the crack generation under thermal condition. The NMC442 was constructed with different grain orientations (Figure 11(B)), where generated mismatch strains, resulting in the production

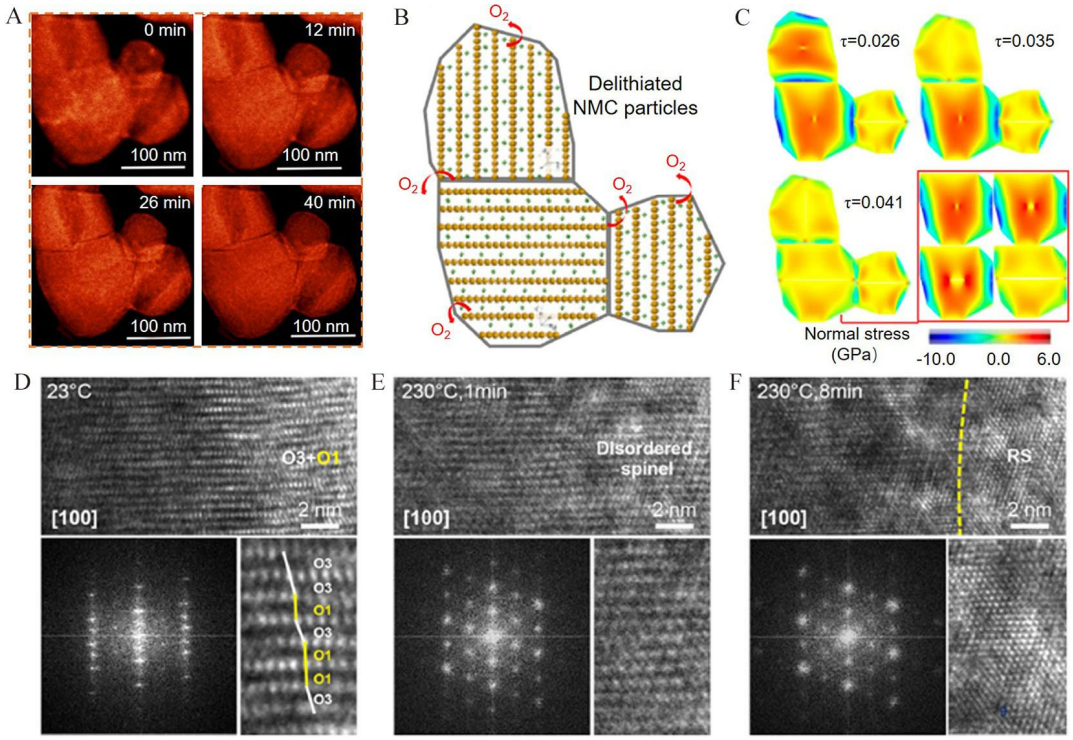

Figure 11 (A) STEM images of NMC442 at 230 °C for 0 min, 12 min, 26 min and 40 min. (B) the constructed FEM model for NMC442 particle. (C) structure evolution of NMC442 particle caused by the oxygen release. Reproduced with permission of Ref.[90], copyright 2018 American Chemical Society. (D-F) the HRTEM images of $LiNiO_2$ at 230 °C for 0 min, 1 min and 8 min. Reproduced with permission of Ref.[91], copyright 2021 Cell Press. (color on line)

and propagation of cracks, accompanied with the O_2 release. Significantly, the O_2 release produced abundant oxygen vacancies in the surface of NMC442, which induced the compressive stress field near the surface, while the tensile stress at the center (Figure 11(C)). Finally, the stress originated from the oxygen loss caused the crack propagation and breakdown of the whole cathode materials.

Mu's work has built a good link between the oxygen release and the crack generation. However, the phase transformation during the thermal conditions should also be further clarified. Wang et al. used the *in situ* high-resolution TEM (HRTEM) to detailly analyze the phase evolution of Ni-rich cathode material employing $LiNiO_2$ as a representative Ni-rich cathode[91]. With the rise of temperature, the oxygen loss gradually aggravated, accompanied by the transition from the layered to the spinel and then to the rock salt phases (Figure 11(D-F)). Furthermore, the evolution path of O1 phase under thermal runaway conditions at the atomic scale was also revealed using the in situ HRTEM. Consistent with the previous reports, the O1 phase was transformed into the rock-salt structure caused by the oxygen release. Different from the transformation of O3 phase, the stepwise transformation pathways were observed. An initial cation mixing and following shear displacement along the (003) planes induced the generation of rock-salt phase. It should be noted that the energy barrier in O1 phase was lower than O3 phase, which accelerated the production of rock-salt phase. In summary, abundant efforts have been put into the research on the relation of the NMC material structure evolution, oxygen release and the thermal stability. However, the practical battery with both high energy density and high safety still needs deeper study to understand the thermal runaway mechanism.

5 Strategies for Ni-Rich Cathode Modification

Above issues greatly hinder the further development of Ni-rich cathode. In order to improve electrochemical performances, several strategies have been adopted to modify the pristine Ni-rich layered oxides for more stable cycling stability and higher capacity including heterogeneous ion doping, coating layer design, morphological control, and concentration gradient regulation. These methods would be briefly discussed in this section.

Proper heteroatom doping in Ni-rich layered oxides can improve the structural stability, reduce the degree of cation mixing and improve the thermal stability[92-94]. Ideally, the doping element should have similar ionic radius to the replaced element, avoiding excessive lattice distortion. In addition, the strong bonding energy with oxygen is expected, which can decrease the release of oxygen during the cycling process. High stability is also necessary, aiming to minimize side reaction. According to these demands, the commonly used elements contain Al[95], Mg[96], Ti[97], Cr[98], F[99] and so on. Huang et al. replaced partial Li by Na in NMC622 through solid phase routine under high temperature[100]. The XRD refinement patterns and DFT results demonstrated that Na^+ doping can effectively inhibit cation mixing in NMC622. Meanwhile, due to the larger radius of Na^+ than Li^+, Na^+ doping can expand the lattice space, which can facilitate Li^+ transport, leading to high initial columbic efficiency, and enhanced cycling and rate performances. In transition metal site doping, Kim et al. compared the produced effect in NMC using Mn, Al, B, W and Ta doping[101]. Differently oriented microstructure was produced with different doping elements, the synthesized $LiNi_{0.90}Co_{0.09}Ta_{0.01}O_2$ delivered a small capacity attenuation rate of only 10% after 2000 cycles and a high energy density more than 850 $Wh \cdot kg^{-1}$. The addition of Ta hindered the coarsening of the particles, thus allowing the best grain refinement within the lithification temperature range. DFT calculation indicated that Ta reduced the surface energy of (003), inducing the strengthened growth of (003), which prevented the generation of Li/Ni mixing at a certain degree. Finally, the doping of anion also produces some performance improvements. The anion always serves as the electron donator, therefore, F^- was used to dope the NMC due to its higher electronegativity than O^{2-} (3.98 vs. 3.44) and the enhanced electrochemical perfor-

mance was achieved[102]. In addition, Cl^- was also employed due to its ability to lose electrons more easily than O^{2-}, thus by improved cycling and rate performances[103].

The design of coating layer is a simple and effective method to suppress the drawbacks of NMC materials, which can block the direct contact of the active material and outer electrolyte, thus avoiding the serious interface issues[104-107]. The coating layer is required to be electrochemically inert in the NMC working voltage range as well as high stability when immersed in the electrolyte. In current reports, metal oxides[108], phosphate[109] and fluorides[110] are commonly used in the coating layer design. Yan et al. introduced Li_3PO_4 coating layer onto the grain boundaries using atomic layer deposition[68]. The Li_3PO_4 coating not only alleviated the fracture of secondary particles and the spinel phase transformation, but also improved the cathode-electrolyte interface dynamics, resulting in the excellent cycling stability.

In the cycling process, the insertion and extraction of Li^+ can only be carried out along the two-dimensional channel in the lithium layer. Therefore, only the {010} crystal planes can effectively exchange Li^+ with the electrolyte[23,111]. The previous works reported that the exposed {010} active planes were beneficial to the rate performance of NMC[112]. However, Hua et al. demonstrated that the frequently-used co-precipitation reaction for NMC synthetization tended to gen erate the (001) plane growth, restraining the growth of {010} planes due to the high surface energy[113]. As a result, it is still challenging for the chosen plane synthetization.

The core-shell structure construction relying on the concentration gradient regulation can produce the NMC materials with high-capacity Ni-rich core and high-stability Mn-rich shell[114-116]. This core-shell structure design not only can suppress the shortcoming of pure Ni-rich NMC, but also eliminate the mismatch between the transition metal components and the traditional coating layer, inducing the stable and fast Li^+ transport in the whole NMC[117]. Kim et al. developed a NMC622 cathode with transitional metal ion concentration gradient in primary particles [31]. This concentration gradient design inhibited the phase transition and the release of oxygen on the sur face during the cycling process. In addition, the contact between the high oxidation state metal ion and the electrolyte was also prevented, thus improving the cyclic performance, and thermal stability.

Apart from the individual modification strategy, the combination of different modification methods is also reported to be effectively suppressing the structure attenuation of NMC cathode. The single modification strategy can only partially address issues of NMC, while dual-modification technique can realize multi-purpose performance improvement. Yang et al. have designed a dual-modification strategy simultaneously combining the cation substitution (La and Ti) and the surface coating (Ti-doped and La_4NiLiO_8)[118]. The coated conductive La_4NiLiO_8 enhanced the surface chemical stability and improved the interfacial kinetic. The doping modification restrained the cation-mixing and relieved the phase transformation. As a result, the synergistic effect obviously improved the cycling stability and capacity of NMC811 cathode.

6 Summary and Outlook

Ni-rich NMC cathode has become one of the most important research topics in the field of lithium-ion batteries. In this review, the research progresses of the structural failure of NMC in practical implementation are summarized in detail, including the internal structure evolution, surface structure evolution and the thermal stability, as well as the strategies to improve its durability: (1) heterogeneous ion doping, (2) coating layer design, (3) morphological control and (4) concentration gradient regulation. Researchers have intensively explored the correlations between the structural behaviors and the performances of Ni-rich NMC cathodes. The territory of structural characterization can be further expanded in the following aspects:

1) Development of advanced *in-situ* characterization techniques: XRD, SEM, TEM, XAS, XPS, FTIR, etc. have made great contributions on the investigation of the structure-performance correlations

of the NMC materials. Advanced *in-situ* techniques can provide unique information for the emerging electrode material exploration on the reaction mechanism, degradation process, and kinetic research. Evolution of key features such as phase, morphology, grain size, facet and valence states can be also directly obtained from these approaches. It should be noted that the current in-situ tests mostly focus on the NMC material itself, whereas the dynamic relations with external electrolyte/anode are often neglected. New *in-situ* technologies are necessary for deeper understanding of the working mechanisms. Building an *in-situ* cell intimating the real reaction condition and measuring electric parameters in real time can be the key feature for an ideal *in-situ* technique where different techniques may require different considerations.

2) Investigation of the structure-function correlation in a full cell at practical conditions: limited by the current technical issues, the recognitions on the reaction mechanism of NMC cathode are often based on the half cell with metallic Li as an anode. This cell has a limited loading, and different power ranges, which is not consistent with the working environment of other types of LIBs. It is critical to observe the structure-function relationship of NMC materials in a full cell with the standardized assembly process and parameters in terms of active material loading mass, electrolyte amounts, etc.

3) Development of simulation tools: understanding on the NMC working and degradation mechanism is fatal for the accurate modification of NMC, which can be realized under the help of theoretical calculations at different scales including the DFT, FEM and machine learning. In addition, high throughput screening can facilitate the search for the emerging electrode materials. In recent studies, the combination of theoretical calculation and experimental analysis has become increasingly close, which derives abundant reasonable directions. However, the normalized criterions should be constructed to prevent calculations from becoming tools that cater to the experimental results.

At the current stage, the research of battery materials is prompted and driven by practical applications. But then, understanding degradation mechanism is of importance for developing not only Ni-rich NMC but also other types of cathode materials. Advanced structural characterizations may provide determining information for understanding the mechanism, and thus, helping design next next-generation LIBs.

Acknowledgements

We acknowledge the supports from the National Natural Science Foundation of China (No. 22075317) and the Strategic Priority Research Program (B) (No. XDB07030200) of Chinese Academy of Sciences.

References:

[1] Jung S K, Hwang I, Chang D, Park K Y, Kim S J, Seong W M, Eum D, Park J, Kim B, Kim J, Heo J H, Kang K. Nanoscale phenomena in lithium-ion batteries[J]. Chem. Rev., 2020, 120(14): 6684-6737.

[2] Xue W, Huang M, Li Y, Zhu Y G, Gao R, Xiao X, Zhang W, Li S, Xu G, Yu Y, Li P, Lopez J, Yu D, Dong Y, Fan W, Shi Z, Xiong R, Sun C J, Hwang I, Lee W K, Shao H Y, Johnson J A, Li J. Ultra-high-voltage Ni-rich layered cathodes in practical Li metal batteries enabled by a sulfonamide-based electrolyte[J]. Nat. Energy, 2021, 6: 495-505.

[3] Manthiram A. A reflection on lithium-ion battery cathode chemistry[J]. Nat. Commun., 2020, 11(1): 1550.

[4] Or T, Gourley S W D, Kaliyappan K, Yu A, Chen Z W. Recycling of mixed cathode lithium-ion batteries for electric vehicles: Current status and future outlook[J]. Carbon Energy, 2020, 2(1): 6-43.

[5] Liu Y, Zhai Y P, Xia Y Y, Li W, Zhao D Y. Recent progress of porous materials in lithium-metal batteries[J]. Small Structures, 2021, 2(5): 2000118.

[6] Li Y, Wu F, Qian J, Zhang M H, Yuan Y X, Bai Y, Wu C. Metal chalcogenides with heterostructures for high-performance rechargeable batteries[J]. Small Science, 2021, 1(9): 2100012.

[7] Gong D C, Wei C Y, Liang Z W, Tang Y B. Recent advances on sodium-ion batteries and sodium dual-ion batteries: State-of-the-art Na^+ host anode materials[J]. Small Science, 2021, 1(6): 2100014.

[8] Zuo W H, Luo M Z, Liu X S, Wu J, Liu H D, Li J, Winter M, Fu R Q, Yang W L, Yang Y. Li-rich cathodes for rechargeable Li-based batteries: Reaction mechanisms and

advanced characterization techniques[J]. Energ. Environ. Sci., 2020, 13(12): 4450-4497.

[9] Qiao Y, Yang H J, Chang Z, Deng H, Li X, Zhou H S. A high-energy-density and long-life initial-anode-free lithium battery enabled by a Li_2O sacrificial agent[J]. Nat. Energy, 2021, 6(6): 653-662.

[10] Zheng J X, Ye Y K, Liu T C, Xiao Y G, Wang C M, Wang F, Pan F. Ni/Li disordering in layered transition metal oxide: Electrochemical impact, origin, and control[J]. Accounts Chem. Res., 2019, 52(8): 2201-2209.

[11] Wu J X, Cao Y L, Zhao H M, Mao J F, Guo Z P. The critical role of carbon in marrying silicon and graphite anodes for high-energy lithium-ion batteries[J]. Carbon Energy, 2019, 1(1): 57-76.

[12] Yu L, Wang J, Xu Z J. A perspective on the behavior of lithium anodes under a magnetic field[J]. Small Structures, 2020, 2(1): 2000043.

[13] Song Y W, Peng Y Q, Zhao M, Lu Y, Liu J N, Li B Q, Zhang Q. Understanding the impedance response of lithium polysulfide symmetric cells[J]. Small Science, 2021: 2100042.

[14] Zhao S Q, Guo Z Q, Yan K, Wan S W, He F R, Sun B, Wang G X. Towards high-energy-density lithium-ion batteries: Strategies for developing high-capacity lithium-rich cathode materials[J]. Energy Storage Mater., 2021, 34: 716-734.

[15] Li T Y, Yuan X Z, Zhang L, Song D T, Shi K Y, Bock C. Degradation mechanisms and mitigation strategies of nickel-rich NMC-based lithium-ion batteries[J]. Electrochem. Energy Rev., 2019, 3(1): 43-80.

[16] Li J, Hwang S, Guo F M, Li S, Chen Z W, Kou R H, Sun K, Sun C J, Gan H, Yu A P, Stach E A, Zhou H, Su D. Phase evolution of conversion-type electrode for lithium ion batteries[J]. Nat. Commun., 2019, 10(1): 2224.

[17] Ren J C, Huang Y L, Zhu H, Zhang B H, Zhu H K, Shen S H, Tan G Q, Wu F, He H, Lan S, Xia X H, Liu Q. Recent progress on MOF-derived carbon materials for energy storage[J]. Carbon Energy, 2020, 2(2): 176-202.

[18] Zhang X D, Yue F S, Liang J Y, Shi J L, Li H, Guo Y G. Structure design of cathode electrodes for solid-state batteries: Challenges and progress[J]. Small Structures, 2020, 1(3): 2000042.

[19] Meng X Y, Sun Y F, Yu M Z, Wang Z Y, Qiu J S. Hydrogen-bonding crosslinking mxene to highly robust and ultralight aerogels for strengthening lithium metal anode [J]. Small Science, 2021, 1(9): 2100021.

[20] Hou P Y, Yin J M, Ding M, Huang J Z, Xu X J. Surface/interfacial structure and chemistry of high-energy nickel-rich layered oxide cathodes: Advances and perspectives[J]. Small, 2017, 13(45): 1701802.

[21] Duffner F, Kronemeyer N, Tübke J, Leker J, Winter M, Schmuch R. Post-lithium-ion battery cell production and its compatibility with lithium-ion cell production infrastructure[J]. Nat. Energy, 2021, 6(2): 123-134.

[22] Cai W, Yan C, Yao Y X, Xu L, Xu R, Jiang L L, Huang J Q, Zhang Q. Rapid lithium diffusion in order@disorder pathways for fast-charging graphite anodes[J]. Small Structures, 2020, 1(1): 2000010.

[23] Chen L, Su Y F, Chen S, Li N, Bao L Y, Li W K, Wang Z, Wang M, Wu F. Hierarchical $Li_{1.2}Ni_{0.2}Mn_{0.6}O_2$ nanoplates with exposed {010} planes as high-performance cathode material for lithium-ion batteries[J]. Adv. Mater., 2014, 26(39): 6756-6760.

[24] Lee S Y, Park G S, Jung C, Ko D S, Park S Y, Kim H G, Hong S H, Zhu Y, Kim M. Revisiting primary particles in layered lithium transition-metal oxides and their impact on structural degradation[J]. Adv. Sci., 2019, 6(6): 1800843.

[25] Nitta N, Wu F, Lee J T, Yushin G. Li-ion battery materials: Present and future[J]. Mater. Today, 2015, 18(5): 252-264.

[26] Bhuvaneswari S, Varadaraju U V, Gopalan R, Prakash R. Structural stability and superior electrochemical performance of Sc-doped $LiMn_2O_4$ spinel as cathode for lithium ion batteries[J]. Electrochim. Acta, 2019, 301: 342-351.

[27] Galceran M, Guerfi A, Armand M, Zaghib K, Casas C M. The critical role of carbon in the chemical delithiation kinetics of $LiFePO_4$[J]. J. Electrochem. Soc., 2020, 167(7): 070538.

[28] Alsamet M A M M, Burgaz E. Synthesis and characterization of nano-sized $LiFePO_4$ by using consecutive combination of sol-gel and hydrothermal methods[J]. Electrochim. Acta, 2021, 367: 137530.

[29] Bai Y, Li L M, Li Y, Chen G H, Zhao H C, Wang Z H, Wu C, Ma H Y, Wang X Q, Cui H Y, Zhou J. Reversible and irreversible heat generation of NCA/Si-C pouch cell during electrochemical energy-storage process[J]. J. Energy Chem., 2019, 29: 95-102.

[30] Xia S B, Huang W J, Shen X, Liu J M, Cheng F X, Liu J J, Yang X F, Guo H. Rearrangement on surface structures by boride to enhanced cycle stability for $LiNi_{0.80}Co_{0.15}Al_{0.05}O_2$ cathode in lithium ion batteries[J]. J. Energy Chem., 2020, 45: 110-118.

[31] Kim J, Cho H, Jeong H Y, Ma H, Lee J, Hwang J, Park M, Cho J. Self-induced concentration gradient in nickel-rich cathodes by sacrificial polymeric bead clusters for high-energy lithium-ion batteries[J]. Adv. Energy Mater.,

2017, 7(12): 1602559.

[32] Li H, Zhou P F, Liu F M, Li H X, Cheng F Y, Chen J. Stabilizing nickel-rich layered oxide cathodes by magnesium doping for rechargeable lithium-ion batteries[J]. Chem. Sci., 2019, 10(5): 1374-1379.

[33] Liang C P, Kong F T, Longo R C, Zhang C X, Nie Y F, Zheng Y P, Cho K. Site-dependent multicomponent doping strategy for Ni-rich $LiNi_{1-2y}Co_yMn_yO_2$ (y = 1/12) cathode materials for Li-ion batteries[J]. J. Mater. Chem. A, 2017, 5(48): 25303-25313.

[34] Li W, Erickson E M, Manthiram A. High-nickel layered oxide cathodes for lithium-based automotive batteries[J]. Nat. Energy, 2020, 5(1): 26-34.

[35] Kim U H, Kim J H, Hwang J Y, Ryu H H, Yoon C S, Sun Y K. Compositionally and structurally redesigned high-energy Ni-rich layered cathode for next-generation lithium batteries[J]. Mater. Today, 2019, 23: 26-36.

[36] Sun H H, Ryu H H, Kim U H, Weeks J A, Heller A, Sun Y K, Mullins C B. Beyond doping and coating: Prospective strategies for stable high-capacity layered Ni-rich cathodes[J]. ACS Energy Lett., 2020, 5(4): 1136-1146.

[37] Li J Y, Manthiram A. A comprehensive analysis of the interphasial and structural evolution over long-term cycling of ultrahigh-nickel cathodes in lithium-ion batteries[J]. Adv. Energy Mater., 2019, 9(45): 1902731.

[38] Liu W, Oh P, Liu X, Lee M J, Cho W, Chae S, Kim Y, Cho J. Nickel-rich layered lithium transition-metal oxide for high-energy lithium-ion batteries[J]. Angew. Chem. Int. Edit., 2015, 54(15): 4440-4457.

[39] Li H Y, Liu A R, Zhang N, Wang Y Q, Yin S, Wu H H, Dahn J R. An unavoidable challenge for Ni-rich positive electrode materials for lithium-ion batteries[J]. Chem. Mater., 2019, 31(18): 7574-7583.

[40] Li Y, Li X H, Wang Z X, Guo H J, Wang J X. Spray pyrolysis synthesis of nickel-rich layered cathodes $LiNi_{1-2x}Co_x$-Mn_xO_2 (x = 0.075, 0.05, 0.025) for lithium-ion batteries[J]. J. Energy Chem., 2018, 27(2): 447-450.

[41] Liu Y, Tang L B, Wei H X, Zhang X H, He Z J, Li Y J, Zheng J C. Enhancement on structural stability of Ni-rich cathode materials by *in-situ* fabricating dual-modified layer for lithium-ion batteries[J]. Nano Energy, 2019, 65: 104043.

[42] Kim U H, Ryu H H, Kim J H, Mü cke R, Kaghazchi P, Yoon C S, Sun Y K. Microstructure-controlled Ni-rich cathode material by microscale compositional partition for next-generation electric vehicles[J]. Adv. Energy Mater., 2019, 9(15): 1803902.

[43] Zhang L Q, Zhu C X, Yu S C, Ge D H, Zhou H S. Status and challenges facing representative anode materials for rechargeable lithium batteries[J]. J. Energy Chem., 2022, 66: 260-294.

[44] Liang L W, Zhang W H, Zhao F, Denis D K, Zaman F U, Hou L R, Yuan C Z. Surface/interface structure degradation of Ni-rich layered oxide cathodes toward lithium-ion batteries: Fundamental mechanisms and remedying strategies[J]. Adv. Mater. Inter., 2019, 7(3): 1901749.

[45] Hu D Z, Su Y F, Chen L, Li N, Bao L Y, Lu Y, Zhang Q Y, Wang J, Chen S, Wu F. The mechanism of side reaction induced capacity fading of Ni-rich cathode materials for lithium ion batteries[J]. J. Energy Chem., 2021, 58: 1-8.

[46] Lin Q Y, Guan W H, Zhou J B, Meng J, Huang W, Chen T, Gao Q, Wei X, Zeng Y W, Li J X, Zhang Z. Ni-Li anti-site defect induced intragranular cracking in Ni-rich layer-structured cathode[J]. Nano Energy, 2020, 76: 105021.

[47] Lee W, Muhammad S, Sergey C, Lee H, Yoon J, Kang Y M, Yoon W S. Advances in the cathode materials for lithium rechargeable batteries[J]. Angew. Chem. Int. Ed., 2020, 59(7): 2578-2605.

[48] Nam K W, Bak S M, Hu E Y, Yu X Q, Zhou Y N, Wang X, Wu L, Zhu Y, Chung K Y, Yang X Q. Combining in situ synchrotron X-ray diffraction and absorption techniques with transmission electron microscopy to study the origin of thermal instability in overcharged cathode materials for lithium-ion batteries[J]. Adv. Funct. Mater., 2013, 23(8): 1047-1063.

[49] Yin S Y, Deng W T, Chen J, Gao X, Zou G Q, Hou H S, Ji X B. Fundamental and solutions of microcrack in Ni-rich layered oxide cathode materials of lithium-ion batteries[J]. Nano Energy, 2021, 83: 105854.

[50] Qian G N, Zhang J, Chu S Q, Li J Z, Zhang K, Yuan Q X, Ma Z F, Pianetta P, Li L S, Jung K, Liu Y J. Understanding the mesoscale degradation in nickel-rich cathode materials through machine-learning-revealed strain-redox decoupling[J]. ACS Energy Lett., 2021, 6(2): 687-693.

[51] Tang Z F, Wang S, Liao J Y, Wang S, He X D, Pan B C, He H Y, Chen C H. Facilitating lithium-ion diffusion in layered cathode materials by introducing Li^+/Ni^{2+} antisite defects for high-rate Li-ion batteries[J]. Research, 2019: UNSP2198906.

[52] Xu Z R, Jiang Z R, Kuai C G, Xu R , Qin C D, Zhang Y, Rahman M M, Wei C X, Nordlund D, Sun C J, Xiao X H, Du X W, Zhao K J, Yan P F, Liu Y J, Lin F. Charge distribution guided by grain crystallographic orientations in polycrystalline battery materials[J]. Nat. Commun., 2020, 11(1): 83.

[53] Su Y F, Zhang Q Y, Chen L, Bao L Y, Lu Y, Chen S, Wu F. Stress accumulation in Ni-rich layered oxide cathodes: Origin, impact, and resolution[J]. J. Energy Chem., 2022, 65: 236-253.

[54] Yoon C S, Ryu H H, Park G T, Kim J H, Kim K H, Sun Y K. Extracting maximum capacity from Ni-rich Li[$Ni_{0.95}Co_{0.025}Mn_{0.025}$]$O_2$ cathodes for high-energy-density lithium-ion batteries[J]. J. Mater. Chem. A, 2018, 6(9): 4126-4132.

[55] Park S Y, Baek W J, Lee S Y, Seo J A, Kang Y S, Koh M, Kim S H. Probing electrical degradation of cathode materials for lithium-ion batteries with nanoscale resolution[J]. Nano Energy, 2018, 49: 1-6.

[56] Cheng X P, Li Y H, Cao T C, Wu R, Wang M M, Liu H, Liu X Q, Lu J X, Zhang Y F. Real-time observation of chemomechanical breakdown in a layered nickel-rich oxide cathode realized by *in situ* scanning electron microscopy[J]. ACS Energy Lett., 2021, 6(5): 1703-1710.

[57] Wu H Q, Qin C D, Wang K, Han X, Sui M L, Yan P F. Revealing two distinctive intergranular cracking mechanisms of Ni-rich layered cathode by cross-sectional scanning electron microscopy[J]. J. Power Sources, 2021, 503: 230066.

[58] Xu Z R, Rahman M M, Mu L Q, Liu Y J, Lin F. Chemomechanical behaviors of layered cathode materials in alkali metal ion batteries[J]. J. Mater. Chem. A, 2018, 6(44): 21859-21884.

[59] Ryu H H, Park K J, Yoon C S, Sun Y K. Capacity fading of Ni-rich Li[$Ni_xCo_yMn_{1-x-y}$]O_2 ($0.6 \leqslant x \leqslant 0.95$) cathodes for high-energy-density lithium-ion batteries: Bulk or surface degradation?[J]. Chem. Mater., 2018, 30(3): 1155-1163.

[60] Miller D J, Proff C, Wen J G, Abraham D P, Bareño J. Observation of microstructural evolution in Li battery cathode oxide particles by *in situ* electron microscopy[J]. Adv. Energy Mater., 2013, 3(8): 1098-1103.

[61] Zheng S Y, Hong C Y, Guan X Y, Xiang Y X, Liu X S, Xu G L, Liu R, Zhong G M, Zheng F, Li Y X, Zhang X Y, Ren Y, Chen Z H, Amine K, Yang Y. Correlation between long range and local structural changes in Ni-rich layered materials during charge and discharge process[J]. J. Power Sources, 2019, 412: 336-343.

[62] Yan P F, Zheng J M, Gu M, Xiao J, Zhang J G, Wang C M. Intragranular cracking as a critical barrier for high-voltage usage of layer-structured cathode for lithium-ion batteries[J]. Nat. Commun., 2017, 8; 14101.

[63] Zhang H L, Omenya F, Yan P F, Luo L L, Whittingham M S, Wang C M, Zhou G W. Rock-salt growth-induced (003) cracking in a layered positive electrode for Li-ion batteries[J]. ACS Energy Lett., 2017, 2(11): 2607-2615.

[64] Xiao B W, Wang K, Xu G L, Song J H, Chen Z H, Amine K, Reed D, Sui M L, Sprenkle V, Ren Y, Yan P F, Li X L. Revealing the atomic origin of heterogeneous Li-ion diffusion by probing Na[J]. Adv. Mater., 2019, 31(29): 1805889.

[65] Li S, Yao Z P, Zheng J M, Fu M S, Cen J J, Hwang S, Jin H L, Orlov A, Gu L, Wang S, Chen Z W, Su D. Direct observation of defect-aided structural evolution in a nickel-rich layered cathode[J]. Angew. Chem. Int. Ed., 2020, 59(49): 22092-22099.

[66] Qian G N, Zhang Y T, Li L S, Zhang R X, Xu J M, Cheng Z J, Xie S J, Wang H, Rao Q L, He Y S, Shen Y B, Chen L W, Tang M, Ma Z F. Single-crystal nickel-rich layered-oxide battery cathode materials: Synthesis, electrochemistry, and intra-granular fracture[J]. Energy Storage Mater., 2020, 27: 140-149.

[67] Trevisanello E, Ruess R, Conforto G, Richter F H, Janek J. Polycrystalline and single crystalline ncm cathode materials-quantifying particle cracking, active surface area, and lithium diffusion[J]. Adv. Energy Mater., 2021, 11(18): 2003400.

[68] Yan P F, Zheng J M, Liu J, Wang B Q, Cheng X P, Zhang Y F, Sun X L, Wang C M, Zhang J G. Tailoring grain boundary structures and chemistry of Ni-rich layered cathodes for enhanced cycle stability of lithium-ion batteries[J]. Nat. Energy, 2018, 3(7): 600-605.

[69] Li Y W, Li Z B, Chen C, Yang K, Cao B, Xu S Y, Yang N, Zhao W G, Chen H B, Zhang M J, Pan F. Recent progress in Li and Mn rich layered oxide cathodes for Li-ion batteries[J]. J. Energy Chem., 2021, 61: 368-385.

[70] Shao M C, Shang C S, Zhang F X, Xu Z, Hu W, Lu Q Q, Gai L G. Selective adsorption-involved formation of NMC532/PANI microparticles with high ageing resis tance and improved electrochemical performance[J]. J. Energy Chem., 2021, 54: 668-679.

[71] Qiu Q Q, Yuan S S, Bao J, Wang Q C, Yue X Y, Li X L, Wu X J, Zhou Y N. Suppressing irreversible phase transition and enhancing electrochemical performance of Ni-rich layered cathode $LiNi_{0.9}Co_{0.05}Mn_{0.05}O_2$ by fluorine substitution[J]. J. Energy Chem., 2021, 61: 574-581.

[72] Wu F, Liu N, Chen L, Li N, Dong J Y, Lu Y, Tan G Q, Xu M Z, Cao D Y, Liu Y F, Chen Y B, Su Y F. The nature of irreversible phase transformation propagation in nickel-rich layered cathode for lithium-ion batteries[J]. J. Energy Chem., 2021, 62: 351-358.

[73] Lin F, Markus I M, Nordlund D, Weng T C, Asta M D,

Xin H L, Doeff M M. Surface reconstruction and chemical evolution of stoichiometric layered cathode materials for lithium-ion batteries[J]. Nat. Commun., 2014, 5: 3529.

[74] Jung S K, Gwon H, Hong J, Park K Y, Seo D H, Kim H, Hyun J, Yang W, Kang K. Understanding the degradation mechanisms of $LiNi_{0.5}Co_{0.2}Mn_{0.3}O_2$ cathode material in lithium ion batteries[J]. Adv. Energy Mater., 2014, 4(1): 1300787.

[75] Tsutomu O, Atsushi U, Nagayama M. Electrochemistry and structural chemistry of $LiNiO_2$ ($R\bar{3}m$) for 4 volt secondary lithium cells[J]. J. Electrochem. Soc., 1993, 140(7): 1862-1870.

[76] Lin Q Y, Guan W H, Meng J, Huang W, Wei X, Zeng Y W, Li J X, Zhang Z. A new insight into continuous performance decay mechanism of Ni-rich layered oxide cathode for high energy lithium ion batteries[J]. Nano Energy, 2018, 54: 313-321.

[77] Wang J, Lu X, Zhang Y, Zhou J, Wang J, Xu S. A new insight into continuous performance decay mechanism of Ni-rich layered oxide cathode for high energy lithium ion batteries[J]. Nano Energy, 2018, 54: 313-321.

[78] Zhang S S. Understanding of performance degradation of $LiNi_{0.80}Co_{0.10}Mn_{0.10}O_2$ cathode material operating at high potentials[J]. J. Energy Chem., 2020, 41: 135-141.

[79] Xu C, Marker K, Lee J, Mahadevegowda A, Reeves P J, Day S J, Groh M F, Emge S P, Ducati C, Layla Mehdi B, Tang C C, Grey C P. Bulk fatigue induced by surface reconstruction in layered Ni-rich cathodes for Li-ion batteries[J]. Nat. Mater., 2021, 20(1): 84-92.

[80] Li W D, Song B H, Manthiram A. High-voltage positive electrode materials for lithium-ion batteries[J]. Chem. Soc. Rev., 2017, 46(10): 3006-3059.

[81] Zhang Y, Katayama Y, Tatara R, Giordano L, Yu Y, Fraggedakis D, Sun J G, Maglia F, Jung R, Bazant M Z, Shao H Y. Revealing electrolyte oxidation via carbonate dehydrogenation on Ni-based oxides in Li-ion batteries by in situ fourier transform infrared spectroscopy[J]. Energ Environ. Sci., 2020, 13(1): 183-199.

[82] Giordano L, Karayaylali P, Yu Y, Katayama Y, Maglia F, Lux S, Shao H Y. Chemical reactivity descriptor for the oxide-electrolyte interface in Li-ion batteries[J]. J. Phys. Chem. Lett., 2017, 8(16): 3881-3887.

[83] Zheng J X, Liu T C, Hu Z X, Wei Y, Song X H, Ren Y, Wang W D, Rao M M, Lin Y, Chen Z H, Lu J, Wang C M, Amine K, Pan F. Tuning of thermal stability in layered $Li(Ni_xMn_yCo_z)O_2$[J]. J. Am. Chem. Soc., 2016, 138 (40): 13326-13334.

[84] Lin Y, Zhou M, Tai X L, Li H F, Han X, Yu J G. Analytical transmission electron microscopy for emerging advanced materials[J]. Matter, 2021, 4(7): 2309-2339.

[85] Zhang S C(张世超), Shen Z Y(沈泽宇), Lu Y Y(陆盈盈). Research progress of thermal runaway and safety for lithium metal batteries[J]. Acta Phys. -Chim. Sin.(物理化学学报), 2020, 37: 2008065.

[86] Noh H J, Youn S, Yoon C S, Sun Y K. Comparison of the structural and electrochemical properties of layered $Li[Ni_xCo_yMn_z]O_2$ (x = 1/3, 0.5, 0.6, 0.7, 0.8 and 0.85) cathode material for lithium-ion batteries[J]. J. Power Sources, 2013, 233: 121-130.

[87] Bak S M, Nam K W, Chang W, Yu X, Hu E, Hwang S, Stach E A, Kim K B, Chung K Y, Yang X Q. Correlating structural changes and gas evolution during the thermal decomposition of charged $Li_xNi_{0.8}Co_{0.15}Al_{0.05}O_2$ cathode materials[J]. Chem. Mater., 2013, 25(3): 337-351.

[88] Li Y, Liu X, Wang L, Feng X N, Ren D S, Wu Y, Xu G L, Lu L G, Hou J X, Zhang W F, Wang Y L, Xu W Q, Ren Y, Wang Z F, Huang J Y, Meng X F, Han X B, Wang H W, He X M, Chen Z H, Amine K, Ouyang M G. Thermal runaway mechanism of lithium-ion battery with $LiNi_{0.8}Mn_{0.1}Co_{0.1}O_2$ cathode materials[J]. Nano Energy, 2021, 85: 105878.

[89] Alvarado J, Wei C X, Nordlund D, Kroll T, Sokaras D, Tian Y C, Liu Y J, Doeff M M. Thermal stress-induced charge and structure heterogeneity in emerging cathode materials[J]. Mater. Today, 2020, 35: 87-98.

[90] Mu L Q, Lin R L, Xu R, Han L L, Xia S H, Sokaras D, Steiner J D, Weng T C, Nordlund D, Doeff M M, Liu Y J, Zhao K J, Xin H L L, Lin F. Oxygen release induced chemomechanical breakdown of layered cathode materials[J]. Nano Lett., 2018, 18(5): 3241-3249.

[91] Wang C Y, Han L L, Zhang R, Cheng H, Mu L Q, Kisslinger K, Zou P C, Ren Y, Cao P H, Lin F, Xin H L. Resolving atomic-scale phase transformation and oxygen loss mechanism in ultrahigh-nickel layered cathodes for cobalt-free lithium-ion batteries[J]. Matter, 2021, 4(6): 2013-2026.

[92] Lv H J, Li C L, Zhao Z K, Wu B R, Mu D B. A review: Modification strategies of nickel-rich layer structure cathode (Ni ⩾ 0.8) materials for lithium ion power batteries[J]. J. Energy Chem., 2021, 60: 435-450.

[93] Yan W W, Yang S Y, Huang Y Y, Yang Y, Yuan G H. A review on doping/coating of nickel-rich cathode materials for lithium-ion batteries[J]. J. Alloy. Compd., 2020, 819: 153048.

[94] Zhang S D(张思东), Liu Y(刘园), Qi M Y(祁慕尧), Cao A M(曹安民). Localized surface doping for improved

stability of high energy cathode materials[J]. Acta Phys.-Chim. Sin. (物理化学学报), 2020, 37: 2011007.

[95] Zhao W G, Zou L F, Jia H P, Zheng J M, Wang D H, Song J H, Hong C Y, Liu R, Xu W, Yang Y, Xiao J, Wang C M, Zhang J G. Optimized al doping improves both interphase stability and bulk structural integrity of Ni-rich NMC cathode materials[J]. ACS Appl. Energ. Mater., 2020, 3(4): 3369-3377.

[96] Yu H F, Zhu H W, Yang Z F, Liu M M, Jiang H, Li C Z. Bulk Mg-doping and surface polypyrrole-coating enable high-rate and long-life for Ni-rich layered cathodes[J]. Chem. Eng. J., 2021, 412: 128625.

[97] Zhang D K, Liu Y, Wu L W, Feng L W, Jin S L, Zhang R, Jin M L. Effect of Ti ion doping on electrochemical performance of Ni-rich $LiNi_{0.8}Co_{0.1}Mn_{0.1}O_2$ cathode material [J]. Electrochim. Acta, 2019, 328: 135086.

[98] Choi J U, Voronina N, Sun Y K, Myung S T. Recent pro gress and perspective of advanced high-energy Co-less Ni-rich cathodes for Li-ion batteries: Yesterday, Today, and Tomorrow[J]. Adv. Energy Mater., 2020, 10(42): 2002027.

[99] Zhao Z Y, Huang B, Wang M, Yang X W, Gu Y J. Facile synthesis of fluorine doped single crystal Ni-rich cathode material for lithium-ion batteries[J]. Solid State Ionics, 2019, 342: 115065.

[100] Huang Z J, Wang Z X, Jing Q, Guo H J, Li X H, Yang Z H. Investigation on the effect of Na doping on structure and Li-ion kinetics of layered $LiNi_{0.6}Co_{0.2}Mn_{0.2}O_2$ cathode material[J]. Electrochim. Acta, 2016, 192: 120-126.

[101] Kim U H, Park G T, Son B K, Nam G W, Liu J, Kuo L Y, Kaghazchi P, Yoon C S, Sun Y K. Heuristic solution for achieving long-term cycle stability for Ni-rich layered cathodes at full depth of discharge[J]. Nat. Energy, 2020, 5(11): 860-869.

[102] Binder J O, Culver S P, Pinedo R, Weber D A, Friedrich M S, Gries K I, Volz K, Zeier W G, Janek J. Investigation of fluorine and nitrogen as anionic dopants in nickel-rich cathode materials for lithium-ion batteries[J]. ACS Appl. Mater. Inter., 2018, 10(51): 44452-44462.

[103] Li X L, Kang F Y, Shen W C, Bai X D. Improvement of structural stability and electrochemical activity of a cathode material $LiNi_{0.7}Co_{0.3}O_2$ by chlorine doping[J]. Electrochim. Acta, 2007, 53(4): 1761-1765.

[104] Li J Y, Yang M X, Huang Z C, Zhao B Q, Zhang G, Li S M, Cui Y H, Dong Z H, Liu H. Nanoscale operation of Ni-rich cathode surface by polycrystalline solid electrolytes $Li_{32}Zr_{04}Si_{06}O_{36}$ coating[J]. Chem. Eng. J., 2021, 417: 129217.

[105] Li Y Y, Li X F, Hu J H, Liu W, Sari H M K, Li D J, Sun Q, Kou L, Tian Z Y, Shao L, Zhang C, Zhang J J, Sun X L. ZnO interface modified $LiNi_{0.6}Co_{0.2}Mn_{0.2}O_2$ toward boosting lithium storage[J]. Energy Environ. Mater., 2020, 3(4): 522-528.

[106] Cheng X P, Zheng J M, Lu J X, Li Y H, Yan P F, Zhang Y F. Realizing superior cycling stability of Ni-rich layered cathode by combination of grain boundary engineering and surface coating[J]. Nano Energy, 2019, 62: 30-37.

[107] Su Y F(苏岳锋), Zhang Q Y(张其雨), Chen L(陈来), Bao L(包丽颖), Lu Y(卢赟), Chen S(陈实), Wu F(吴锋). Effects of ZrO_2 coating on Ni-rich $LiNi_{08}Co_{01}Mn_{01}O_2$ cathodes with enhanced cycle stabilities[J]. Acta Phys.-Chim. Sin. (物理化学学报), 2020, 37(3): 2005062.

[108] Li Y, Liu X, Ren D S, Hsu H J, Xu G L, Hou J X, Wang L, Feng X N, Lu L G, Xu W Q, Ren Y, Li R H, He X M, Amine K, Ouyang M G. Toward a high-voltage fast-charging pouch cell with TiO_2 cathode coating and enhanced battery safety[J]. Nano Energy, 2020, 71: 104643.

[109] Gan Q M, Qin N, Wang Z Y, Li Z Q, Zhu Y H, Li Y Z, Gu S, Yuan H M, Luo W, Lu L, Xu Z H, Lu Z G. Revealing mechanism of Li_3PO_4 coating suppressed surface oxygen release for commercial Ni-rich layered cathodes [J]. ACS Appl. Energ. Mater., 2020, 3(8): 7445-7455.

[110] Dai S C, Yan G J, Wang L, Luo L M, Li Y P, Yang Y T, Liu H H, Liu Y, Yuan M L. Enhanced electrochemical performance and thermal properties of Ni-rich $LiNi_{0.8}Co_{0.1}Mn_{0.1}O_2$ cathode material via CaF_2 coating[J]. J. Electroanal. Chem., 2019, 847: 113197.

[111] Zhang L J, Li N, Wu B R, Xu H L, Wang L, Yang X Q, Wu F. Sphere-shaped hierarchical cathode with enhanced growth of nanocrystal planes for high-rate and cycling-stable Li-ion batteries[J]. Nano Lett., 2015, 15(1): 656-661.

[112] Su Y F, Chen G, Chen L, Li W K, Zhang Q Y, Yang Z R, Lu Y, Bao L Y, Tan J, Chen R J, Chen S, Wu F. Exposing the {010} planes by oriented self-assembly with nanosheets to improve the electrochemical performances of Ni-rich $Li[Ni_{0.8}Co_{0.1}Mn_{0.1}]O_2$ microspheres[J]. ACS Appl. Mater. Inter., 2018, 10(7): 6407-6414.

[113] Hua W B, Liu W Y, Chen M Z, Indris S, Zheng Z, Guo X D, Bruns M, Wu T H, Chen Y X, Zhong B H, Chou S L, Kang Y M, Ehrenberg H. Unravelling the growth mechanism of hierarchically structured $Ni_{1/3}Co_{1/3}Mn_{1/3}(OH)_2$ and their application as precursors for high-power cathode materials[J]. Electrochim. Acta, 2017, 232: 123-131.

[114] Li Y C, Xiang W, Xiao Y, Wu Z G, Xu C L, Xu W, Xu

Y D, Wu C, Yang Z G, Guo X D. Synergy of doping and coating induced heterogeneous structure and concentration gradient in Ni-rich cathode for enhanced electrochemical performance[J]. J. Power Sources, 2019, 423: 144-151.

[115] Park N Y, Ryu H H, Park G T, Noh T C, Sun Y K. Optimized Ni-rich NCMA cathode for electric vehicle batteries[J]. Adv. Energy Mater., 2021, 11(9): 2003767.

[116] Wu K, Wang J Y, Li Q, Yang Y Q, Deng X, Dang R B, Wu M M, Wu Z J, Xiao X L, Yu X Q. *In situ* synthesis of a nickel concentration gradient structure of Ni-rich $LiNi_{0.8}Co_{0.15}Al_{0.05}O_2$ with promising superior electrochemical properties at high cut-off voltage[J]. Nanoscale, 2020, 12(20): 11182-11191.

[117] Sun Y K, Chen Z, Noh H J, Lee D J, Jung H G, Ren Y, Wang S, Yoon C S, Myung S T, Amine K. Nanostructured high-energy cathode materials for advanced lithium batteries[J]. Nat. Mater., 2012, 11(11): 942-947.

[118] Yang H, Wu H H, Ge M, Li L, Yuan Y, Yao Q, Chen J, Xia L, Zheng J, Chen Z, Duan J, Kisslinger K, Zeng X C, Lee W K, Zhang Q, Lu J. Simultaneously dual modification of Ni-rich layered oxide cathode for high-energy lithium-ion batteries[J]. Adv. Funct. Mater., 2019, 29(13): 1808825.

锂离子电池高镍层状氧化物正极结构失效机制

王加义[1,2],郭胜楠[1],王 新[2*],谷 林[1],苏 东[1*]

(1. 中国科学院物理研究所,北京凝聚态物理国家研究中心,北京 100190;
2. 华南师范大学,信息光电子科技学院,肇庆市华师大光电产业研究院,广州 510006)

摘要: 高镍层状氧化物具有成本低、能量密度高的优点,被认为是新一代锂离子电池的理想正极材料。然而,由于在使用中其结构的耐久性与安全性问题,在实际应用过程中仍然面临着严峻的挑战。深入了解电极材料容量衰减过程中的结构演变对发展高性能层状氧化物电极材料具有重要的指导意义。本文综述了近年来高镍层状氧化物正极失效机理的研究进展,包括从高镍层状氧化物的内部结构演变、表面成分变化和热失控条件下的性质等方面,进行了详细的梳理。之后,本文介绍了国内外最新的高镍层状氧化物的改性策略,并对高镍氧化物正极结构研究的发展方向进行了总结和展望。

关键词: 锂离子电池;正极;高镍层状氧化物;结构失效机制